JOURNAL OF MECHANICAL ENGINEERING AND SCIENCES
ISSN: 2289-4659 e-ISSN: 2231-8380
VOLUME 20, ISSUE 2, 2026, 11209 - 11231
DOI: https://doi.org/10.15282/jmes.20.2.2026.6.0874

RESEARCH ARTICLE

Energy, exergy, and exergoeconomic analysis of a gas turbine plant with integrated waste heat recovery

N. A. Mohd Iskandar[1], A. M. I. Mamat[1,2]*

[1]Faculty of Mechanical Engineering, Universiti Teknologi MARA, 40450, Shah Alam, Selangor Darul Ehsan, Malaysia
[2]Smart Manufacturing Research Institute (SMRI), Universiti Teknologi MARA, 40450, Shah Alam, Selangor Darul Ehsan, Malaysia
Phone: +6035543 5251; Fax.: +6015543 5052

Abstract - Suboptimal thermal efficiency of gas turbine operation is caused by a significant portion of the input energy lost as waste heat. This study investigates the integration of advanced waste heat recovery systems to mitigate these losses, enhance overall plant performance and increase operating revenue. A comprehensive thermodynamic model was developed based on the first and second laws of thermodynamics to simulate a gas turbine integrated with a combined cycle gas turbine, electric turbocompounding and a regenerative cycle. The feasibility of on-site waste-to-hydrogen production from the electrolysis process of the recovered energy was also evaluated. The model was analysed across a range of compressor pressure ratios and combustion chamber temperature rises. For the baseline gas turbine, the maximum exergetic efficiency was 11% at PR_C of 12 and a combustion chamber temperature rises of 1000 K, with efficiency declining at higher compressor pressure ratios. The integrated system with waste heat recovery significantly increased the exergetic efficiency up to 26% at a higher compressor pressure ratios of approximately 12. A preliminary exergoeconomic analysis indicated that the integrated system could reduce electricity fuel costs by up to 50% relative to the baseline plant and generate up to $4,000 per hour in additional revenue stream through on-site production of cost-competitive hydrogen. The results indicate that the strategic integration of multi-stage energy recovery systems can more than double the exergetic efficiency of gas turbine power plants, thereby maximising useful work output and enabling a sustainable thermal system with hydrogen co-production.

Article History
Received : 17 December 2025
Revised : 4 March 2026
Accepted : 21 April 2026
Published : 30 June 2026

Keywords
Gas turbine
Exergy analysis
Exergoeconomic
Waste heat Recovery
Waste-to-Hydrogen

1. Introduction

Gas turbine power plants are widely used for electricity generation due to their higher power output and relatively low emissions compared to other hydrocarbon-fuel-based power plants. However, the thermal efficiency of a gas turbine is often suboptimal because a significant portion of the input energy is lost as waste heat [1]-[2]. To address this problem, researchers have explored various methods to recover waste heat and subsequently improve the overall efficiency of gas turbine systems. This studies the integration of energy recovery systems, such as the steam Rankine cycle (SRC), electric turbocompounding (ETC), and regenerative cycles, into gas turbine power plants. The electrical power generated by the ETC is used to operate an electrolyser for on-site waste-to-hydrogen (WtH). Energy and exergy analyses are essential tools for evaluating the performance of gas turbine power plants [3]. Exergy analysis provides insights into the irreversibilities and losses within the system, enabling the identification of areas for improvement. Mishra and Singh [4] conducted a thermodynamic analysis of combined-cycle gas turbine (CCGT) plants, highlighting the importance of exergy analysis for optimising thermal performance. They found that exergy destruction in the combustion chamber was the primary source of inefficiency, accounting for up to 40% of total losses. Similarly, Reddy et al. [5] reviewed energy and exergy analyses of thermal power plants, emphasising the need for efficient waste heat recovery systems to enhance overall efficiency. Their study showed that integrating CCGT systems could reduce exergy destruction by up to 15%, significantly improving system performance. Despite using thermodynamic modelling, Dai et al. [6] developed an advanced numerical method based on big data analysis to predict gas turbine performance[6]. A neural network method was applied to predict turbine performance degradation, helping the operator plan maintenance, repair, and overhaul.

The integration of waste-heat recovery systems, such as CCGTs, has been widely studied to improve the efficiency of gas turbine power plants. Almutairi et al. [7] demonstrated that the CCGT system could effectively recover low-grade heat from the gas turbine exhaust, thereby significantly enhancing the plant's overall thermal efficiency. Their results showed that the CCGT system could increase the net power output by up to 10% when integrated with a gas turbine. Bhargava et al. [8] investigated the use of CCGT systems in offshore settings, demonstrating that CCGT could improve efficiency across various power ratings. They found that the CCGT system was particularly effective in recovering waste heat from gas turbines with power ratings above 50 MW, achieving exergetic efficiencies of up to 80%. Oyedepo and Fakeye [9] provided a comprehensive overview of the thermodynamics and optimisation of CCGT systems, highlighting their potential to convert waste heat into useful electricity. They emphasised that the choice of working fluid and operating parameters, such as Pressure and temperature, was critical to determining the CCGT system's efficiency. CCGTs, which integrate gas and steam turbines, are known for their high efficiency. Kumar [10] optimised CCGT performance by considering various operating parameters, demonstrating that integrating SRC systems could further enhance efficiency. The results showed that the CCGT system could increase net power output by up to 15%, thereby significantly improving the plant's overall efficiency. Dev et al. [11] developed a model to analyse the efficiency of CCGTs, emphasising the

*CORRESPONDING AUTHOR | A. M. I. Mamat | ✉ amanihsan@uitm.edu.my

importance of optimising pressure ratios and mass flow rates. They found that the optimal pressure ratio for a CCGT ranged from 10 to 15, depending on the specific operating conditions. A higher gas turbine efficiency, h, reduces the exergy cost, $\dot{c}_E$, and the cost of electricity, $\dot{c}_e$. Table 1 summarises the commercial gas turbine performance parameter data sheets published by the gas turbine manufacturers. All the commercial data are accessible online.

Table 1. Commercial gas turbine data sheet performance parameters

Manufacturer	Model	Fuel Type	Compressor Ratio (PRc)	TIT (K)	Heat Rate (kJ/kWh)	Power Output (MW)	Efficiency (%)	Exhaust Flow (kg/s)	Exhaust Temp. (K)	Cost of Exergy ($/GJ)	Fuel Cost, $\dot{c}_e$. ($/MWh)	Exergy Fuel Cost Rate, $\dot{c}_E$. ($/hr)	References
Ansaldo Energia	GT26 / GT36	H_2-blend / Natural gas	20	1773	5,854	288	61.5	1,550	903	$10.74	$102.27	$29,453	[12], [13]
	7EA	Natural Gas	12	-	10,909	87	33	-	-	$2.68	$30.99	$2,697	[14]
	7HA.01/03	Natural Gas	22	1873	5,625	430	64	1,450	883	$2.68	$24.35	$10,471	[15], [16]
General Electric	9F.05	Natural gas/ Diesel	18.5	1673	6,000	440	60	1,200	923	$2.68	$26.21	$11,532	[17]
	LM2500	Natural gas	19	-	9,231	33	39	-	-	$2.68	$26.21	$865	[18]
	LM6000	Natural gas/ Diesel	30	1593	8,571	47	42	250	813	$2.68	$23.79	$1,118	[19]
Kawasaki	M7A-03	Natural gas	15	1473	9,474	18	38	80	793	$2.68	$26.21	$472	[20]
Mitsubishi Heavy Industries	M501JAC	Natural gas	24	1873	5,625	470	64	1,500	883	$2.68	$24.35	$11,445	[21]
	M701F4/5	Natural gas/ Diesel	18	1723	5,806	312	62	1,400	893	$2.68	$25.56	$7,975	[22]
Pratt & Whitney	FT8	Natural gas	23	-	9,231	31	39	-	-	$2.68	$26.21	$812	[23]
Rolls-Royce	RB211	Natural gas/ Diesel	21	1573	9,000	60	40	220	803	$2.85	$24.63	$1,478	[24]
	Trent 60	Diesel	37	-	8,571	64	42	-	-	$2.85	$24.63	$1,576	[25]
Siemens Energy	SGT5-9000HL	Natural gas	22	1823	5,669	545	63.5	1,600	873	$2.68	$24.56	$13,385	[26]
	SGT6-8000H	Natural gas	19	1723	6,000	286	60	1,100	913	$2.68	$26.21	$7,496	[27]

The ETC is another method for recovering waste energy from gas turbine exhaust gases. ETC systems use a low-pressure radial turbine to extract energy from the exhaust stream, which is then converted into electrical power. Zhuge et al. [28] optimised an ETC system for recovering energy from gasoline engine exhaust, demonstrating its potential to improve overall system efficiency. Their results showed that the ETC system could recover up to 5% of the exhaust energy, increasing the net power output by 3-4%. Bălănescu and Homutescu [29] further validated the effectiveness of ETC in gas turbine power plants, showing that it could significantly increase the net power output. They found that the ETC system was most effective at higher pressure ratios, where the exhaust gas energy was sufficient to drive the turbine. However, they also noted that the ETC system added complexity to the gas turbine, potentially increasing maintenance costs.

The use of sustainable fuels, such as hydrogen, in gas turbine power plants has attracted attention as a way to reduce carbon emissions. Blue hydrogen, produced through steam methane reforming with carbon capture and storage (CCS), is a promising lower-carbon alternative to conventional natural gas. Oyedepo and Fakeye [9] investigated the potential of CCGT systems to recover waste heat for hydrogen production, demonstrating that the recovered energy could be utilised to power electrolysers and produce enough hydrogen to replace up to 20% of the natural gas used by the gas turbine. The study of the correlation among energy, exergy, exergoeconomic, and environmental (4E) factors was conducted to evaluate the potential of existing gas turbine power plants to integrate hydrogen systems to improve sustainability [30]-[31]. They found that integrating hydrogen could reduce carbon emissions by up to 30%, making power plants more environmentally friendly [32]. Although hydrogen has a better environmental impact, hydrogen production costs are generally higher than those of hydrocarbon fuels, and production is classified [33]-[34]. The analysis of the levelized cost of hydrogen (LCOH) production is summarised in Table 2. Although the Chlor-Alkali process for producing hydrogen is the cheapest, it depends heavily on Chlorine economics, which are highly unreliable [35]. The LCOH of Grey and Blue hydrogen is competitive with the levelized cost of energy of natural gas, which is approximately $ 1.5 – 3.5 per MMBtu [36]. Currently, several gas turbines use a mixture of traditional hydrocarbon fuels with hydrogen. Arsalis [37] used thermodynamic modelling to investigate the effect of gas turbine performance when fuelled by natural gas-hydrogen. Also, several studies combining methane and hydrogen have found that gas turbine performance improved by up to 15% and that carbon emissions were reduced compared with hydrocarbon fuels [2], [38].

Table 2. Parameters for a baseline of the model

Hydrogen colour	LCOH price	Production site price	Selling price	References
Gray hydrogen (SMR)	$1.0 - $2.5	$2.5 - $4.5	$4.0 - $8.0	[39], [40]
Blue hydrogen (SMR+CCS)	$1.5 - $3.5	$3.0 - $5.5	$5.0 - $9.0	[39], [41]
Green hydrogen (Electrolysis)	$3.0 - $7.0	$4.0 - $8.0	$6.0 - $12.0	[33], [39]
Turquoise hydrogen (Methane pyrolysis)	$2.0 - $4.0	$3.5 - $6.5	$5.5 - $10.0	[34], [42]
Pink hydrogen (Nuclear electrolysis)	$2.5 - $5.5	$3.5 - $6.5	$5.5 - $10.0	[43], [44]
By-product hydrogen (Chlor-alkali)	$0.5 - $2.0	$1.5 - $3.5	$3.5 - $7.0	[35]

Exergy destroyed, which represents the loss of useful work potential due to irreversibilities, is a critical factor in the performance of gas turbine systems. Moliere et al. [45] analysed the exergetic performance of gas turbines under part-load conditions, showing that exergy destroyed increases with higher pressure ratios. They found that exergy destroyed in the combustion chamber was the primary source of inefficiency, accounting for up to 50% of total losses. Khaldi and Adouande [46] conducted an exergy analysis of gas turbine power plants, identifying the combustion chamber as the primary source of exergy destruction, with exergy destruction increasing with combustion temperature. They noted that reducing exergy destroyed in the combustion chamber could significantly improve the plant's overall efficiency. While the previous individual components of waste heat recovery and hydrogen production offer promising pathways, their standalone implementation often faces economic and technical hurdles, including high capital costs, material constraints, and sub-optimal efficiency. This study posits that a holistic, systems-level approach is key to overcoming these barriers. Prior studies have explored CCGT or ETC in isolation; this study is the first to model a triple-stage cascading architecture (CCGT–ETC–RC), in which the ETC serves as the dedicated power source for WtH production. This architecture is designed to maximise exergy recovery in a cascading manner, thereby boosting overall efficiency to a level that may offset the initial investment. By directly linking the ETC's electrical output to hydrogen electrolysis, the model also addresses the challenge of integrating sustainable fuels, creating a closed-loop system that enhances both efficiency and environmental performance. The core objective of this work is to provide a validated thermodynamic framework that demonstrates how such deep integration can make gas turbine plants more economically viable and environmentally sustainable.

2. Materials and Methods

2.1 Gas Turbine Numerical Framework

A numerical model of energy and exergy for an energy recovery system in a gas turbine power plant was developed based on thermodynamic fundamentals. The methodology involved developing a numerical model based on the first and second laws of thermodynamics to evaluate the performance of the gas turbine power plant under various conditions. In the model, each system component was treated as a separate control volume, and most of the equations were obtained from Çengel [47]. Figure 1 shows a flowchart for the gas turbine mathematical modelling. The first and second laws of thermodynamics were used to develop the mathematical model for all components in the gas turbine and energy recovery systems. The overall performance of the gas turbine is evaluated by using the overall thermal efficiency, h and the exergetic efficiency, h_{ii}. The operating conditions of the gas turbine model are presented in Table 3.

2.2 Architecture Model

Modelling and control of gas turbine systems are crucial, interrelated disciplines essential for studying and improving their performance and efficiency. Understanding gas turbine dynamics before actual installation or for existing gas turbine units cannot be achieved without sufficiently accurate models. The primary goals of gas turbine modelling include simulators for training purposes, condition monitoring and fault diagnosis, performance upgrades through control system analysis, and stability studies. Various modifications to the basic gas turbine cycle have been implemented to enhance performance. The gas turbine comprises key components, including compressors, combustion chambers, and turbines. The SRC system utilises the waste heat from the gas turbine to generate additional electricity. The schematic layout of the gas turbine power plant and energy recovery system is shown in Figure 2. An ETC unit is located downstream of the economiser and generates high-pressure steam. The remaining exhaust energy is then recuperated into the regenerator to reduce the combustion exergy. The first and second laws of thermodynamics were used to model the energy and exergy of all components in the gas turbine system, as shown in Figure 2. The thermodynamic process depicted in Figure 2 can be represented in a Temperature-Entropy (T-s) diagram, which illustrates the processes within the system. Figure 3 shows the locations of the states from the schematic layout in Figure 2, and all the properties at each state were derived by obtaining the values of a subset of properties.

Objective		Input		Process		Outcome
Components Modelling		Thermodynamics and combustion	→	Gas turbine model	→	Energy exergy
		Exergy recovery	→	Steam cycle	→	Mechanical recovery
		Electrical power and storage	→	Electric turbocompounding	→	Mechanical recovery and storage
		Exhaust exergy	→	Regenerator	→	Combustion exergy reduction
				⇩		
System Modelling		Energy exergy	→	First & second law cycle efficiency	→	First and second thermal efficiency
		Energy recovery	→	Recovery system	→	Overall performance
		Electrochemical	→	Hydrogen electrolyser	→	Hydrogen production
		Exergoeconomic		Fuel and hydrogen		Cost and revenue

Figure 1. The flowchart of energy and exergy modelling

Table 3. Parameters for a baseline of the model

Parameter's description	Value and unit
Inlet	
Mass flow rate of air (Kg/s)	50 – 500 kg/s
Inlet pressure	1 atm
Inlet temperature	298 K
Compressor	
Stage compression ratio, $PR_{C,i}$	1.05-1.25
Number of rows	3; 5; 7
Sections	2; LPC H; HPC
Combustion chamber	
Fuel	Natural gas (75% CH_3; 15%C_2H_6; 10%N_2)
Temperature change in combustor, DT	800 K; 1000 K; 1200 K
Turbine	
Stage expansion ratio, E$R_{T,i}$	1.2
Number of rows	3; 5
Sections	2; HPT, LPT

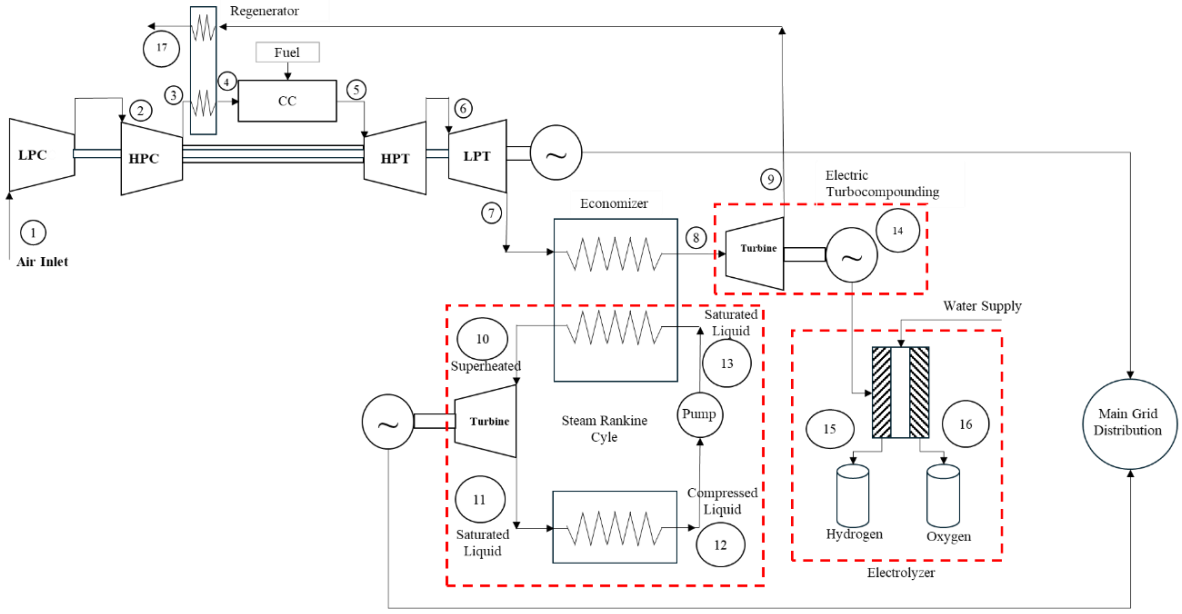

Figure 2. Architecture for a gas turbine power plant with a waste heat recovery system

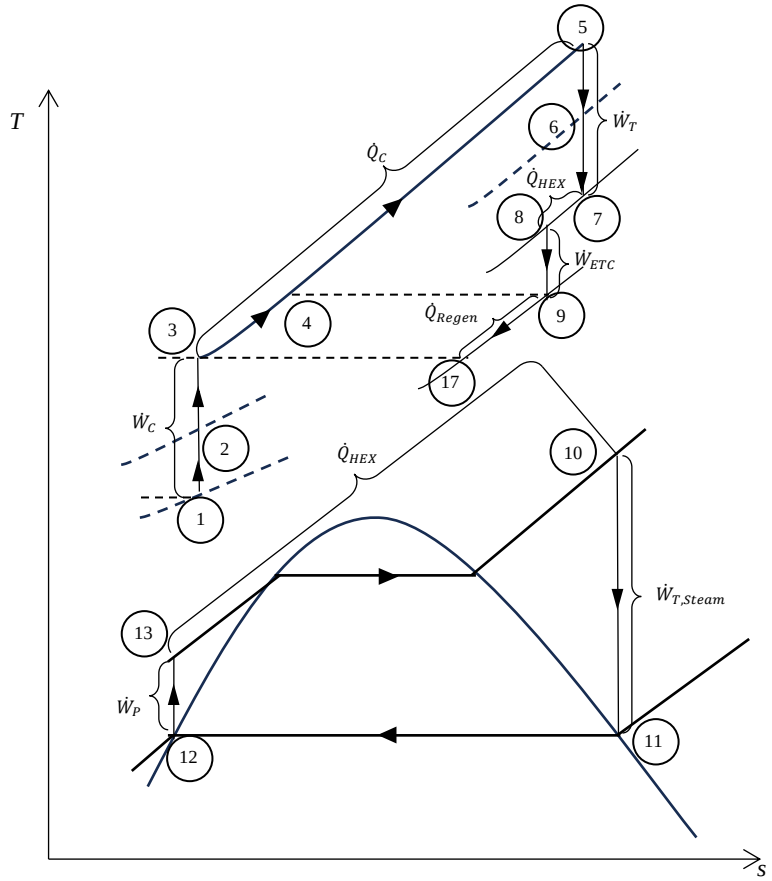

Figure 3. Temperature-entropy diagram for the processes of energy system architecture for a gas turbine power plant with an energy recovery system

2.3 Theoretical Modelling

2.3.1 Compressor Section

The mathematical formulations for energy and exergy analysis are derived from the first and second laws of thermodynamics. The thermodynamic model was used to develop a numerical model simulating the performance of the gas turbine power plant. The isentropic compression work in the compressor, $\dot{W}_C$, is given by Eqs. (1-2).

$$\dot{W}_C = \dot{m}_a C_{p,avg}(T_4 - T_1) \quad (1)$$

where, $C_p(T) = \alpha + \beta T + \delta T^2 + \varepsilon T^3$ (2)

Specific heat at constant pressure, $C_p(T)$, varies with temperature. The modelling set dry air as the working fluid, treated as an ideal gas; thus, $\alpha = 28.11, \beta = 0.1967 \times 10^{-2}, \delta = 0.4802 \times 10^{-5}$, and $\varepsilon = -1.966 \times 10^{-9}$, where the values were obtained from [47]. The relationship between the inlet and outlet temperatures of the compressor is obtained using the isentropic relation given by Eq. (3).

$$\frac{T_3}{T_1} = (PR_C)^{\frac{\gamma-1}{\gamma}} \quad (3)$$

where PR_C is the compression ratio in the compressor, and it is derived from Eq. (4).

$$PR_C = (PR)^{n-1} \quad (4)$$

where n is the number of stages in the compressor that comprises a row of rotors and stators, finally, the rate of exergy destruction in the compressor can be obtained from the steady-state exergy rate balance applied to the compressor, assuming no heat transfer to the surroundings. Eq. (5) takes the form.

$$E_{D,C} = \dot{m}(e_{C,1} - e_{C,3}) - \dot{W}_C \quad (5)$$

where $e_{C,}$ zero accounts for the exergy per unit of mass entering at the compressor inlet, and e_{C4} accounts for the exergy per unit mass at the compressor exit. These terms are known as specific flow exergy and are expressed in Eq. (6).

$$e_C = (h_i - h^\circ) - T^\circ(s_i - s^\circ) \quad (6)$$

where h_i is the enthalpy per unit mass at the state temperature, obtained using Eq. (2); h° is the enthalpy per unit mass at the standard reference state, set at 298 K; s_i and s° is the Entropy at the state temperature and the standard reference temperature, respectively.

2.3.2 Combustion Chamber

The theoretical chemical reaction in a gas turbine combustion chamber primarily involves the combustion of a hydrocarbon fuel (e.g., natural gas, kerosene, or jet fuel) with air to produce high-temperature and high-pressure gases that drive the turbine. The chemical reaction was assumed to be at steady-state combustion, as depicted in Figure 4.

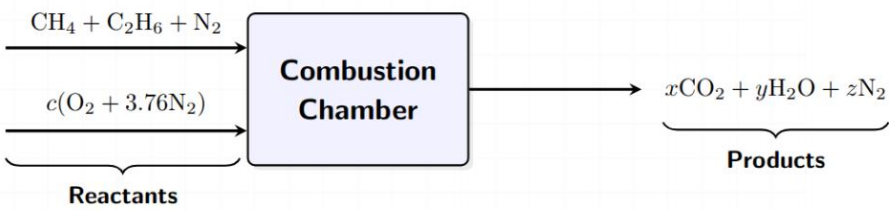

Figure 4. Steady flow combustion

The model assumed a natural gas composition of 75% methane (CH_4), 15% Ethane (C_2H_6), and 5% nitrogen (N_2). The chemical reaction is given by Eq. (7).

$$CH_4 + C_2H_6 + N_2 + 2.025(O_2 + 3.76N_2) \rightarrow 1.05CO_2 + 1.95H_2O + 7.714N_2 \quad (7)$$

The chemical reaction in Eq. (7) can be used to calculate the Air-to-Fuel Ratio (AFR) of the combustion process, as given by Eq. (8).

$$AFR = \frac{m_a}{m_f} = \frac{N_a M_a}{N_f M_f} \quad (8)$$

where m_a is the mass of the air, and m_f is the mass of the fuel. The mass of air and fuel was obtained from the number of moles, N and the Molar Mass of the substance, M. Also, the chemical balance in Eq. (7) can be used to calculate the rate of heat transfer from the combustion process. Equation (9) was derived from the first law of thermodynamics and can be used to calculate the Enthalpy of combustion.

$$\dot{Q}_{Com} = \frac{\dot{m}_f}{M_f}\left\{\sum N_r(\bar{h}^\circ_f + \bar{h} - \bar{h}^\circ)_r - \sum N_p(\bar{h}^\circ_f + \bar{h} - \bar{h}^\circ)_p\right\}(kW\ of\ fuel) \quad (9)$$

where $\bar{h}^\circ_f$ is the Enthalpy of formation, $\bar{h}^\circ$ is the Enthalpy at the standard reference temperature, which is at 298 K, and $\bar{h}$ is the Enthalpy at the state temperature for the combustor inlet (reactants, r) and the combustor outlet (products, p). The Entropy of combustion can be analysed using the second law of thermodynamics for the reacting system, including the combustion chamber surroundings. The total Entropy generated from the combustion process is determined from Eq. (8). Eq. (10) is used to calculate the recovered energy, thereby increasing the gas turbine cycle efficiency.

$$S_{gen} = \frac{1}{M_f}\left\{\sum N_p\left[\bar{s}_i(T,P_0) - \bar{R}_u ln\left(\frac{y_i P_m}{P_0}\right)\right]_p - \sum N_r\left[\bar{s}_i(T,P_0) - \bar{R}_u ln\left(\frac{y_i P_m}{P_0}\right)\right]_r\right\} + \frac{\dot{Q}_{Com}}{\dot{m}_f T_0}\left(\frac{kJ}{kg.K}\right) \quad (10)$$

2.3.3 Turbine

The combustion chamber increases the temperature, and the energy is extracted in the turbine to convert the high Pressure and high temperature into useful mechanical work. The mechanical work is generated by gas expansion. The turbine power generation is given by Eqs. (11)-(13).

$$\dot{W}_T = \dot{m}_g C_{p,avg}(T_{05} - T_{07}) \quad (11)$$

$$\frac{T_7}{T_5} = (ER_T)^{\frac{\gamma-1}{\gamma}} \quad (12)$$

$$ER_T = (ER)^m \quad (13)$$

where $\dot{m}_g$ is the mass flow rate of gas, which is the summation of the mass flow rate of air, $\dot{m}_a$ and the mass flow rate of fuel, $\dot{m}_f$; ER_T is the total gas Expansion Ratio in the turbine, and Eq. (12) was used, where *m* represents the number of stages of expansion in the turbine. Eq. (2) is also used to calculate the $C_{p,avg}$. The mechanical power from the turbine drives both the compressor and the electric generator, as shown in Eq. (14).

$$\dot{W}_{net} = \dot{W}_{T,is} + \dot{W}_{C,is} \quad (14)$$

The gas turbine cycle efficiency, η, can be calculated using Eq. (15), which is the ratio of $\dot{W}_{net}$ in Eq. (14) to $\dot{Q}_{Com}$ in Eq. (9).

$$\eta = \frac{\dot{W}_{net}}{\dot{Q}_{Com}} \quad (15)$$

2.3.4 Exergy Analysis

The amount of recoverable energy can be analysed using the exergy analysis of the gas turbine cycle. The wasted exergy of the gas turbine cycle can be calculated by using the exergy analysis. Eq. (16) provides the amount of exergy destroyed and the corresponding $\dot{E}_{D,C}$ throughout the gas turbine cycle.

$$\dot{E}_{D,C} = \dot{m}_g S_{gen} \quad (16)$$

The exergetic efficiency (η_{II}) is described in Eq. (17).

$$\eta_{II} = \frac{\dot{W}_{net}}{\dot{E}_{in} - \dot{E}_{Out}} \quad (17)$$

where $\dot{E}_{in}$is is the rate of inlet exergy in the combustion process, and $\dot{E}_{Out}$is is the exergy at the exhaust gas outlet.

2.3.5 Steam Rankine Cycle

The numerical modelling has recovered energy that was destroyed by $\dot{E}_{D,Com}$ using the SRC. Water was used as the working fluid in the SRC, and the heat exchanger served as an economiser to recover exhaust heat downstream of the turbine. The compressed water received heat from the exhaust, changing phase from a compressed liquid to superheated vapour. The heat exchange process can be represented by Eq. (18).

$$\dot{E}_{D,Com} = \dot{Q}_{Hex} = \dot{m}_v(h_{10} - h_{13}) \quad (18)$$

where $\dot{m}_v$ is the steam flow rate in the SRC, Eq. (18) shows that the energy recovered by the SRC depends on the enthalpy change, which is highly sensitive to the turbine inlet pressure. The superheated water vapour expands in the turbine, producing mechanical power to drive the electric generator. Eq. (19) is derived from the first law of thermodynamics for the turbine.

$$\dot{W}_{T,Steam} = \dot{m}_v(h_{10} - h_{11}) \quad (19)$$

The SRC utilises a pump to compress the saturated water exiting the condenser into compressed water before it enters the heat exchanger. Eq. (20) was used to calculate the amount of power required by the pump.

$$\dot{W}_P = \dot{m}_v \upsilon(P_{13} - P_{12}) \quad (20)$$

where υ is the specific volume of the water at the pump inlet, P_{12} is the saturated Pressure of the water at the pump inlet, and P_{13} is the exit pressure of the pump.

2.3.6 Electric Turbocompounding

The exhaust gas temperature from the gas turbine will be reduced at the heat exchanger exit; however, the pressure drop across the heat exchanger is not significant. Subsequently, the exhaust exits the heat exchanger as low-quality energy. A high-performance, low-pressure radial turbine can be used in the ETC to extract low-quality energy. In the ETC, a shaft

is connected to drive the electric generator at a higher speed to minimise back Pressure. Eq. (21) was used to calculate the low-pressure radial turbine power output.

$$\dot{W}_{LPT} = \dot{m}_g C_{p,avg}(T_8 - T_9) \tag{21}$$

2.3.7 Regenerative Cycle

The regenerative cycle (RC) improves the gas turbine by using a heat exchanger (regenerator) to preheat the compressed air before it enters the combustion chamber, thereby reducing fuel consumption. In this study, the regenerator utilises the waste heat from the ETC, and its Regenerator effectiveness ε_{Regen} was assumed to be 70% [48]. Eq. (22) was used to obtain preheat temperature, T_4.

$$T_4 = T_3 + \varepsilon_{Regen}\frac{C_{p,9}}{C_{p,4}}(T_9 - T_{17}) \tag{22}$$

2.3.8 Alkaline Hydrogen Electrolyser

The recovered energy from the ETC can be converted into chemical energy stored as hydrogen gas. In an alkaline electrolyser, water is split at the electrodes: hydrogen is produced at the cathode and oxygen at the anode. The chemical reactions at the anode and cathode are presented in Eqs. (23) and (24).

Anode: $H_2O \rightarrow 2H^+ + 0.5O_2 + 2e^-$ (23)

Cathode: $2H^+ + 2e^- \rightarrow H_2$ (24)

The overall chemical reaction in the electrolyser is given by Eq. (25).

$$H_2O + P_E \rightarrow H_2 + 0.5O_2 \tag{25}$$

where the P_E is the electrical power supply to the electrolyser, obtained from the $\dot{W}_{LPT}$. The total available received by the Hydrogen electrolysis stack is given by Eq. (26).

$$\dot{W}_{Stack} = \dot{W}_{LPT} - \dot{W}_{BoP} - \dot{W}_{Comp,H_2} \tag{26}$$

where $\dot{W}_{BoP}$ is ower consumed by Balance-of-Plant such as pumps, cooling, purification which is typically modelled as a percentage of the stack power for 10% of the total power [49]. $\dot{W}_{Comp,H_2}$ is the power consumed by the H_2 compressor, and in this study, the H_2 compression ratio, $PR_{H2,}$ was assumed at 700. Then, Eq. (26) can be used to determine the number of moles of hydrogen produced during electrolysis.

$$n_{H2} = \eta_F \frac{\dot{W}_{LP}}{2FP_E} \tag{27}$$

where F is the Faraday constant, which is 96485 C/mol, and P_E is the voltage of the electrolysis operating condition. This model assumes P_E = 1.8 V for ideal electrolysis operation. $\eta_F$is the Faradaic efficiency, which was assumed at 99% [50]. Thus, the mass flow rate of hydrogen, $\dot{m}_{H_2}$, can be obtained in Eq. (28).

$$\dot{m}_{H_2} = \frac{n_{H2}M_{H2}}{3600s} \tag{28}$$

where M_{H2} is the Molar mass of hydrogen (2 kMol/kg), the electrolysis is supplied by water, and Eq. (29) can be used to determine the water flow rate, $\dot{m}_{H_2O}$.

$$\dot{m}_{H_2O} = \frac{n_{H_2O}M_{H_2O}}{3600s} \tag{29}$$

where M_{H_2O} is the Molar mass of H_2O, which is 18 kMol/kg.

2.3.9 Exergoeconomic Modelling

The effectiveness of the gas turbine thermal system utilising the energy can be translated into economic activity. Exergoeconomic analysis evaluates the direct economic implications of exergy flows within the system. The $\dot{c}_E$ for 1 MWhr of natural gas fuel is given by Eq. (30), obtained from [32].

$$\dot{c}_E = \frac{\dot{E}_{GT}p_{NG}}{E} \tag{30}$$

where E is the exergy conversion per MCF, which is 1.183 GJ/MCF; in this study, the Natural gas fuel cost, p_{NG}, was set at $3.00 per MCF [51]. The cost of energy, $\dot{c}_e$ to generate electrical energy, $\dot{W}_E$ from the gas turbine system, is given in Eq. (31).

$$\dot{c}_e = \frac{\dot{c}_E}{\dot{W}_E} \tag{31}$$

Revenue from hydrogen production can be calculated using Equation (32).

$$\dot{R}_{H_2} = \dot{m}_{H_2} p_{H_2} \tag{32}$$

where p_{H_2} is the price of hydrogen, which was set at $2.5/kg [51]

3. Results and Discussion

The formulations integrated into the gas turbine and energy recovery modelling will be analysed and presented in accordance with the system layout. Initial results from the energy and exergy analyses of gas turbine components, including the compressor, combustion chamber, and turbine, will be presented. Then, the effects of energy recovery systems, such as CCGT, ETC, and RC, are analysed. The performance of commercial gas turbines will also be compared with the theoretical computational method developed in the paper. Thereafter, hydrogen production will be analysed and presented, and the exergoeconomics of the waste heat recovery system and hydrogen production will be evaluated in the final section of this paper.

3.1 Compressor

The compressor section was divided into two sections: the low-pressure compressor (LPC) and the high-pressure compressor (HPC). The compressors were investigated at three-stage conditions: five (5), seven (7), and nine (9). The PR for each stage was set from 1.05 to 1.2 in increments of 0.05. The compressor net exergy, $\dot{E}_C$ and the compressor exergy destroyed, $\dot{E}_D$ C, are given in Figure 5. The $\dot{E}_C$ and $\dot{E}_D$ (C) are depicted on the primary and secondary *y*-axes, respectively. The exergy results were obtained using Eqs. (5) and (6), with a mass flow rate of 200 kg/s. Figure 5 shows that the following trend is similar to that of enthalpy and entropy increasing with temperature, as given in Equation (6). Additionally, the increase in Entropy at higher temperatures has increased $\dot{E}_{D\,C}$ at higher PR_C. Thus, the higher the power input required by the compressor to increase the PR_C, the higher $\dot{E}_{D,C}$.

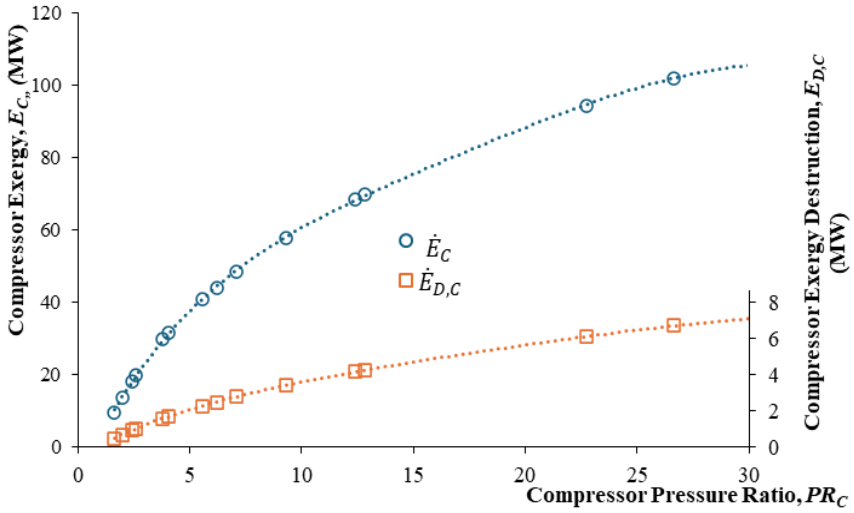

Figure 5. Compressor net exergy and exergy destruction in compressor

3.2 Combustion Chamber

The firing temperature in the combustion chamber is a primary criterion for a high-performance gas turbine. Although a higher firing temperature increases cycle efficiency by producing more mechanical work, it also subjects critical components to thermal fatigue and creep, reducing their service life. In this combustion analysis, the firing temperatures were set at three different temperature changes, ΔT: (1) 800 K, (2) 1000 K, and (3) 1200 K. Eq. (9) was used to calculate the rate of the heat of the combustion process, $\dot{Q}_{Com}$ and the results are depicted in Figure 6. Figure 6 shows that the increase $\dot{Q}_{Com}$ is greater as the ΔT increases because the Enthalpy at the state temperature increases. Additionally, the $\dot{Q}_{Com}$ increase occurs as the PR_C increases due to the higher exit temperature of the compressor section. Figure 6 shows that a higher firing temperature, driven by a higher PR_C, increases the $\dot{Q}_{Com}$.

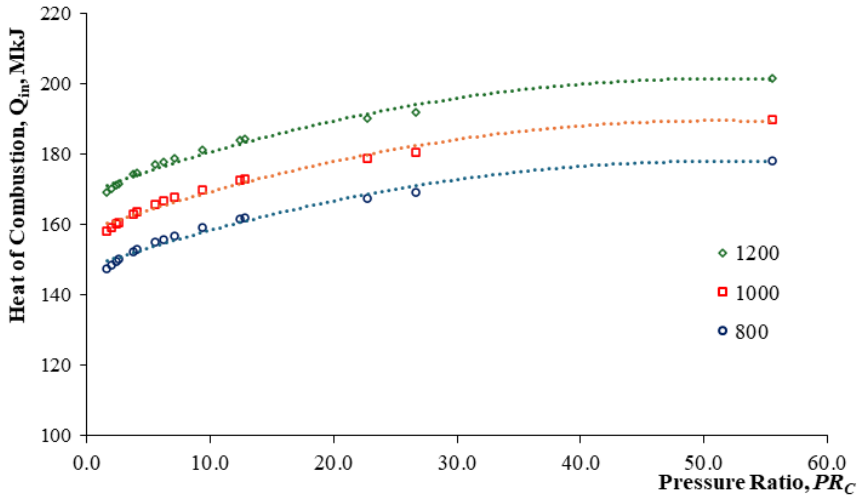

Figure 6. Heat of combustion, $\dot{Q}_{Com}$

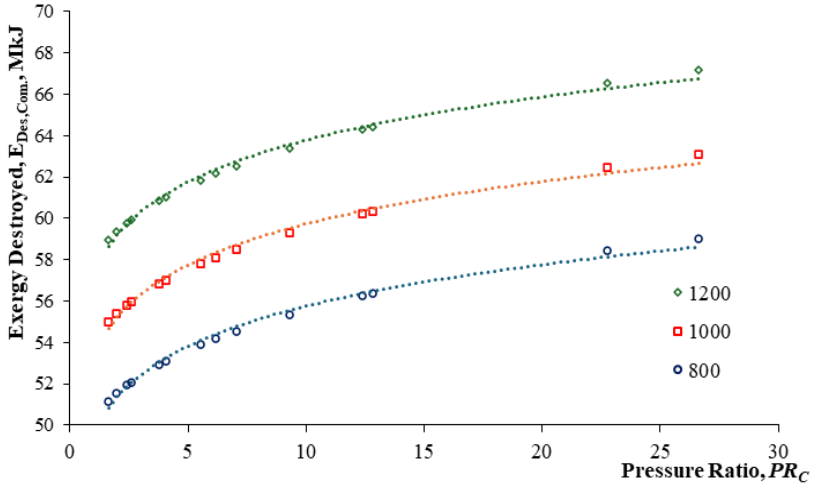

Figure 7. Exergy destroyed, $\dot{E}_{D,Com}$

Combustion exergy destruction represents the loss of the maximum work potential due to irreversibilities inherent in the combustion process. These irreversibilities arise primarily from chemical reaction losses, thermal energy dissipation, incomplete combustion, and molecular mixing and diffusion. During combustion, high-exergy reactants, such as fuel and oxygen, are transformed into low-exergy products, such as carbon dioxide and water, which have significantly less chemical work potential. Additionally, heat generated during combustion is often transferred at a lower temperature than the flame temperature, introducing additional irreversibilities. The total exergy destruction $\dot{E}_{D,Com}$ is quantified as the difference between the exergy entering with the reactants and the exergy leaving with the products, including useful work or heat, or equivalently as $T_0 S_{gen}$, where T_0 is the ambient temperature, and S_{gen} is the entropy generation that was obtained from Eq. (10). Figure 7 shows the $\dot{E}_{D,Com}$ from the combustion process in the combustion chamber for three DTs at various PR_Cs. High exergy destruction indicates significant energy losses, underscoring the need for optimisation strategies such as preheating reactants, improving combustion completeness, and minimising heat losses to enhance system efficiency and performance.

3.3 Turbine

The maximum theoretical work the turbine can produce equals its exergy rate, $\dot{E}_T$. The interaction of high-pressure, hot gases from the combustion chamber drives the turbine rotor, and some of the available energy is converted into useful mechanical work to drive the compressor and the electric generator. Figure 8 shows the $\dot{E}_T$ for five turbine stages. It varies at three (3) DT in the combustion chamber: 800 K, 1000 K, and 1200 K. Higher DT results in significantly higher $\dot{E}_T$ output due to larger enthalpy drops, with 1200 K achieving the highest values (up to ≈200 MW at PR_C =30), followed by 1000 K (≈180 MW) and 800 K (≈160 MW). Figure 8 shows that, although $\dot{E}_T$ it increases with PR_C, the rate of increase diminishes beyond $PR_C \approx 25$, indicating a region of diminishing returns. The presence of 5 turbine stages efficiently distributes energy extraction, minimising losses. Overall, operating at higher inlet temperatures and moderate PR_C is most effective for maximising turbine exergy. Some of the energy will be wasted as heat transfer and destroyed exergy ($\dot{E}_{T,D}$).

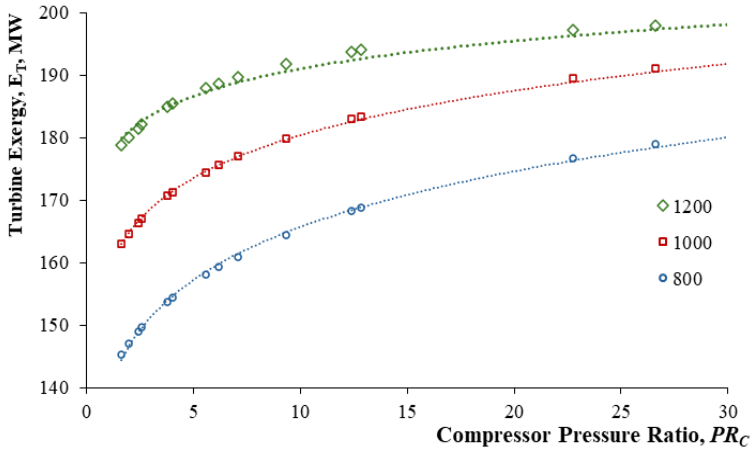

Figure 8. Turbine rate of exergy, $\dot{E}_T$ at various *DT*

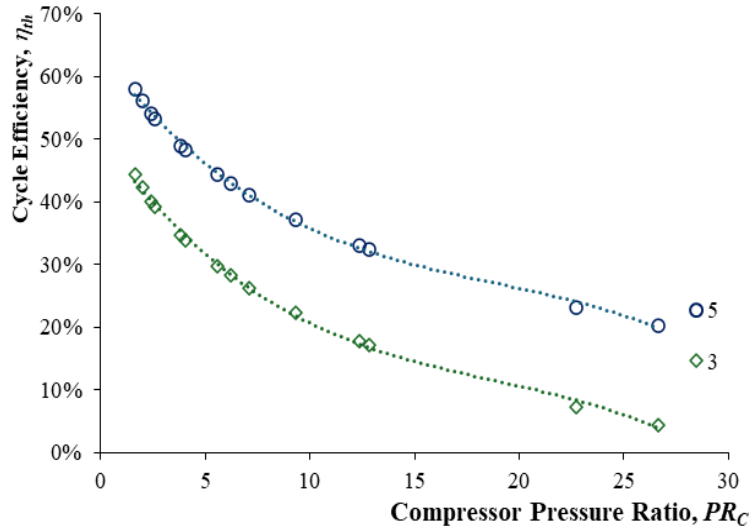

$(a)\eta$ at 3 and 5 turbine stages

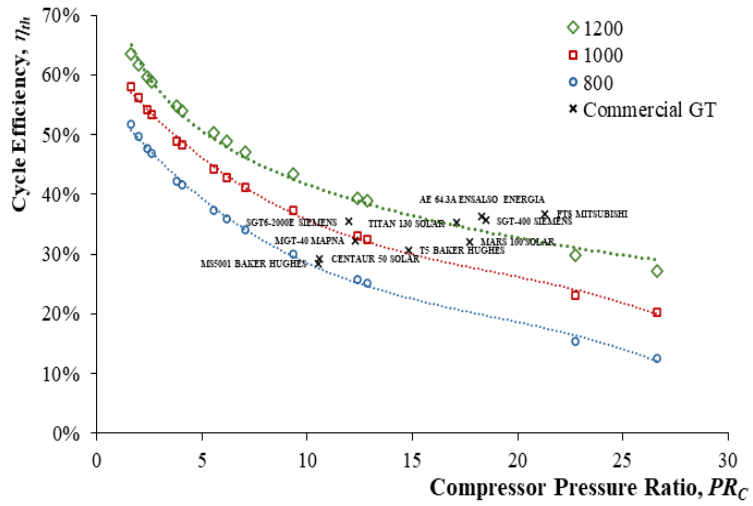

$(b)\eta_{th}$ at 800 K, 100 K and 1200 K and Commercial Gas Turbine [20]

Figure 9. Gas turbine cycle efficiency, η

The W_{Net} represents the useful work from the gas turbine, converted from the $\dot{Q}_{Com}$. The $\dot{W}_{Net}$ to Q_{Com} ratio is denoted η, and the modelling results for three (3) and five (5) turbine stages are shown in Figure 9(a). Initially, the analysis was conducted at a combustion temperature of 1000 K. The η increase in the number of stages is due to the increase in WNet, as shown in Figure 9(a). The maximum of 58% is found at PRC = 1.63 for a turbine stage count of 5. Figure 9(b) shows η at three ΔTs, corresponding to the combustion temperature in the combustion chamber. Figure 12(b) shows that a higher ΔT in the combustion chamber increases η. The increase in η a higher DT is due to a higher turbine inlet temperature,

which has increased the $\dot{W}_{Net}$. Also, the maximum η of 63% is found at ΔT = 1200 K. Despite the increase in the PR_C, which has increased $\dot{Q}_{Com}$ and $W_{T\,out}$ Figure 9(a) shows that $\eta_{th}$is decreases as the PR_C is increased. The decrease is due to the greater energy required to drive the compressor to increase the PR_C; consequently, the $\dot{W}_{Net}$ decreases. Also, Figure 9(b) compares the modelling η with the Commercial Gas Turbine Thermal Efficiency, η_{GT}, obtained from the published data, as shown in Table 1. The η_{GT} matches the modelling of η in this work.

Exergy is destroyed in the turbine due to irreversibilities associated with the expansion of the hot gases to rotate the rotor blades and the temperature difference between the turbine and the surroundings. The Pressure and temperature drop from the expansion process have increased the Entropy. Figure 10 illustrates the exergy destroyed $\dot{E}_{D,T}$ in a turbine as a function of PR_C for three DT: 800 K, 1000 K, and 1200 K. Exergy destruction arise from irreversibilities such as friction, heat transfer, and non-ideal processes, governed by the second law of thermodynamics, where higher entropy generation leads to greater losses. At DT = 800 K, exergy destruction increases with PR_C due to rising irreversibilities, stabilising at higher PR_C, indicating a consistent trend in entropy generation. For DT = 1000 K, exergy destruction peaks at a lower PR_C, then decreases gradually as the pressure ratio increases, suggesting improved efficiency and reduced irreversibilities at higher PR_C. At DT = 1200 K, exergy destruction decreases significantly as PR_C *increases*, indicating that higher inlet temperatures reduce entropy generation and improve the turbine's thermodynamic performance. The principle behind these trends is that higher inlet temperatures increase exergy while reducing the relative impact of irreversibilities, thereby reducing exergy destruction. Additionally, increasing PR_C improves cycle efficiency, but at lower DT (800 K), irreversibilities dominate due to limited energy availability, leading to higher exergy destroyed. In contrast, at higher DT (1200 K), the turbine operates closer to ideal conditions, minimising entropy generation and reducing exergy destruction. Thus, higher inlet temperatures, combined with optimised pressure ratios, are key to reducing exergy losses and enhancing turbine performance.

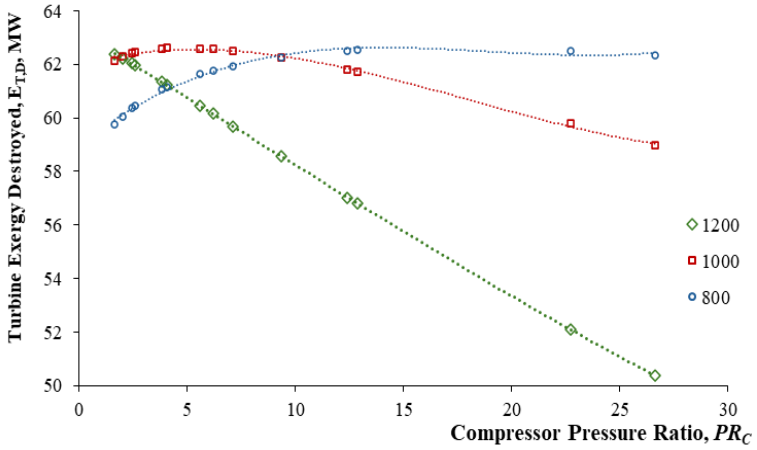

Figure 10. Turbine exergy destroyed, $\dot{E}_{T,D}$

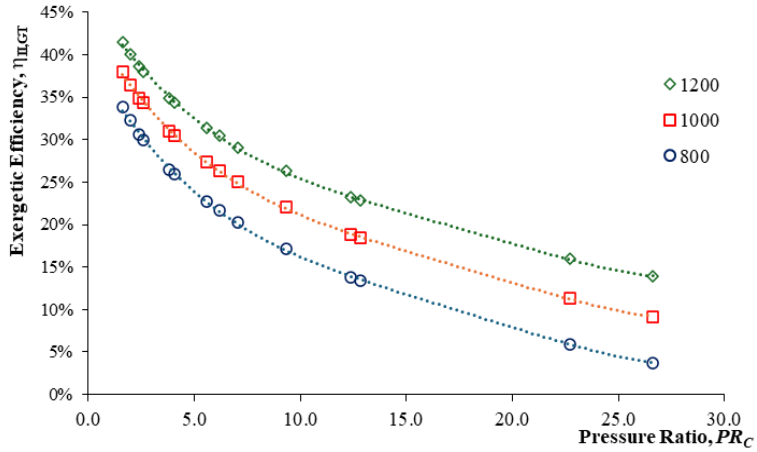

Figure 11. Exergetic efficiency, η_{II}

The exergetic efficiency, η_{II}, provides information on the effectiveness of energy utilisation in converting into useful work. Figure 11 shows the η_{II} for three *DT*s: 800 K, 1000 K, and 1200 K at various PR_C. In general, η_{II} decreases as the PR_C increases, reflecting the greater exergy at higher PR_C. Additionally, Figure 11 shows that η_{II} increases with increasing DT. Many methods can be used to improve energy utilisation through exergy recovery. In this paper, two methods were employed to improve energy conversion. A liquid stream was added to the system via a heat exchanger, and a turbine was installed in the low-pressure exhaust gas. The former is the thermal exchange effect, and the latter is the pressure-expansion effect in energy conversion. The useful recovered energy will be converted into mechanical power output. The effects of the energy recovery are discussed in the next section.

3.4 Waste Energy Recovery

Despite the lower $\dot{E}_{D,T}$ at the higher DT, and the higher PR_C, η_{th} is reduced due to the power required to drive the compressor. A waste heat recovery system can be integrated into the gas turbine power system to increase energy utilisation and, consequently, η_{th}. In this paper, the theoretical model integrates the Combined Cycle Power Plant (CCPP) system with electric turbocompounding. The CCCP modelling is described in section 2.3.5. Additionally, the modelling has simulated hydrogen energy storage using the Hydrogen Electrolysis electrochemical model.

3.4.1 Combine cycle gas turbine

In the CCGT, the hot exhaust gases from the gas turbine are directed to an economiser. The economiser is a heat exchanger that produces steam by exchanging heat with the gas turbine exhaust gas. The steam drives a steam turbine, generating additional power as it expands. The analysis in Figure 12 was conducted for a steam turbine pressure ratio, *PR* of 40. The recovered energy was converted into useful mechanical work, net by the steam turbine, $\dot{W}_{Net,R}$, as depicted in Figure 12 at various PR_C and three *DT*. The $\dot{W}_{Net,R}$ increases as the PR_C and *DT* are increased due to higher $\dot{E}_{D,Com}$.

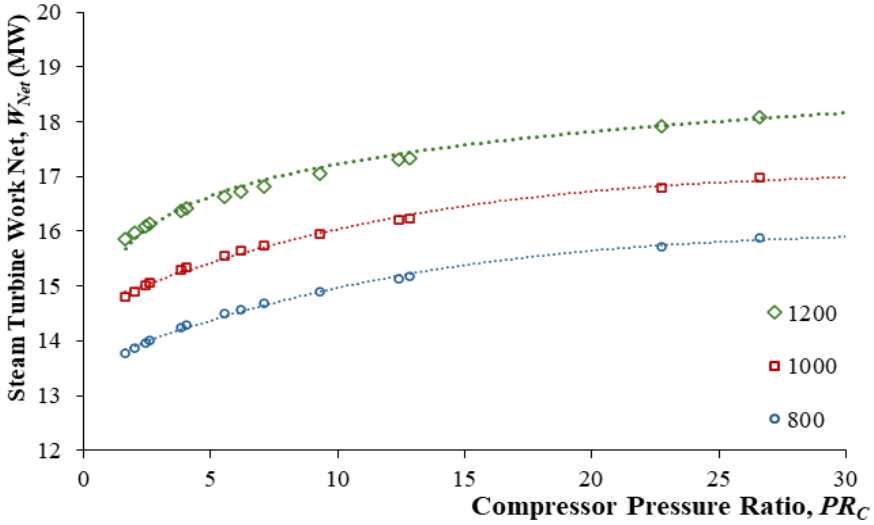

Figure 12. Work net of rankine cycle, $\dot{W}_{Net,R}$ for various compressor pressure ratio, PR_C and combustion temperature change, *DT*

The $\dot{W}_{Net,R}$, is additional power that can be extracted by the steam turbine and used to produce electrical energy for the main grid. The Total Power of the combined cycle, $\dot{W}_{R+GT}$, is the summation of the $\dot{W}_{Net,R}$ and the $\dot{W}_{Net}$. The effectiveness of the energy conversion can be presented as the Cycle Efficiency, h_{R+GT}. Figure 13 shows the effect of the energy recovery from the combined cycle at the *DT* = 1000 K. Despite a similar trend depicted as in Figure 11, where the h_{R+GT} is decreased as the PR_C is increased, Figure 13 shows that the h_{R+GT} is increased as *PR*, is increased because the *Dh* is increased at higher *PR*.

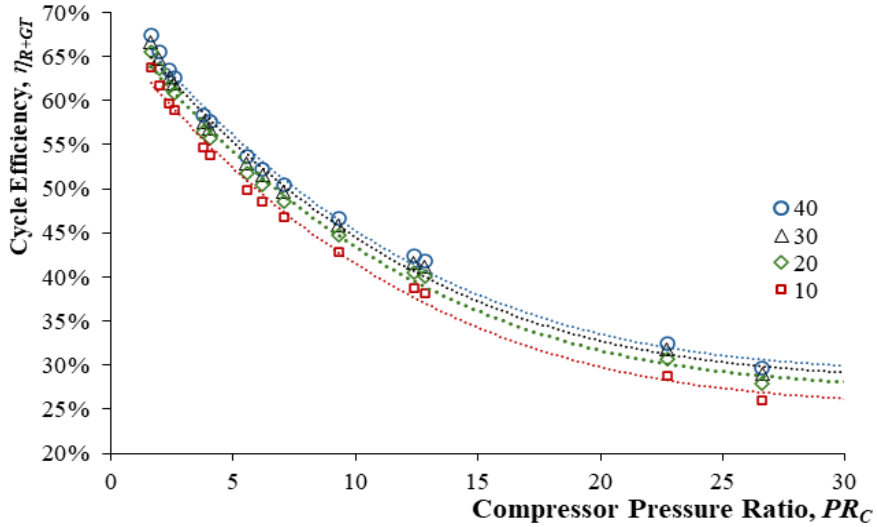

Figure 13. Thermal efficiency of combined rankine and gas turbine cycle, η_{ORC+GT} for various compressor pressure ratio, PR_C and steam turbine pressure ratio, *PR*

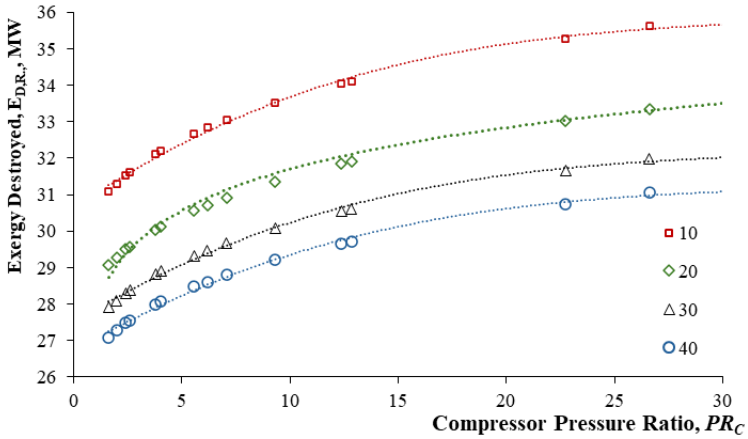

Figure 14. Exergy destroyed in the steam cycle, $\dot{E}_{D,R}$ for various compressor pressure ratios, PR_C and steam turbine pressure ratios, PR

The steam turbine and pump are assumed to operate isentropically. Thus, no entropy is generated during the expansion and compression of the steam turbine and pump, respectively. The entropy destruction, $\dot{E}_{D,R}$, occurs only in the condenser, where heat is exchanged between the surroundings and the steam cycle. The condenser operating pressure was set at 100 kPa. The energy released in the condenser changes the water's phase from saturated vapour to saturated liquid. Figure 14 depicts the $\dot{E}_{D,R}$ Rankine cycle at various PR_C and PR. The $\dot{E}_{D,S}$ is increased due to the PR_C and PR, reflecting the sensitivity of the steam flow rate $\dot{m}_v$.

3.4.2 Electric turbocompounding

The ETC is located downstream of the CCGT heat exchanger. In this numerical study, the back Pressure in the heat exchanger is assumed to be negligible. Figure 15 shows the recovered energy, $\dot{W}_{ETC}$, that the ETC can produce, and the exergy destroyed in the ETC, $E_{ETC,D}$ at various PR_C *for DT=1000 K*. The $\dot{W}_{ETC}$ and $E_{ETC,D}$ are increased, as observed in Figure 15. It can also be observed in Figure 15 that $\dot{W}_{ETC}$ E_{ETC} D are zero when the PR_C is less than 5, because the turbine exit pressure is below standard atmospheric Pressure. Therefore, no energy can be recovered by the ETC; consequently, the ETC cannot operate under these conditions. The amount of recovered $\dot{W}_{ETC}$ is limited at higher PR_C, as shown in Figure 15, where no significant increase occurs after the PR_C exceeds 25. This choking trend is common for the $\dot{E}_{D,ETC}$. Therefore, the operating PR_C should not exceed 25 to avoid choking conditions.

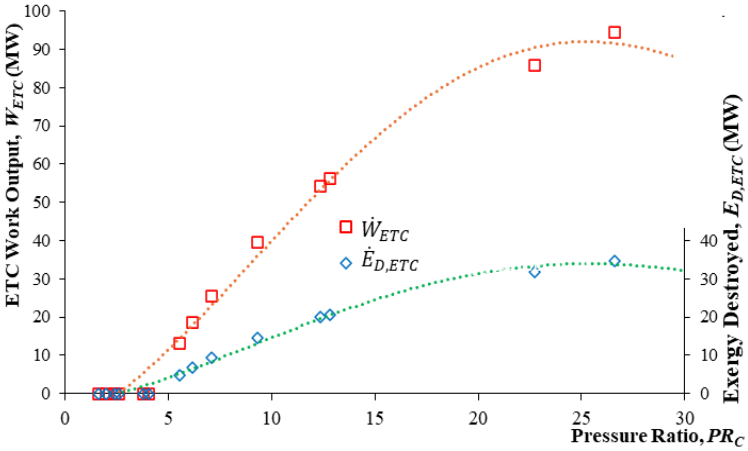

Figure 15. Work output of ETC, $\dot{W}_{ETC}$ & exergy destroyed $E_{ETC,D}$ for various compressor pressure ratios, PR_C

The total work of the system, $\dot{W}_{Net+Steam+ETC}$, is the sum of $\dot{W}_{Net,GT}$, $\dot{W}_{Net,R}$, and $\dot{W}_{ETC}$. Figure 16 depicts the amount of $\dot{W}_{Net+R+ETC}$ at various PR_Cs and PRs. Figure 16 shows that $\dot{W}_{Net+R+ETC}$it increases with increasing PR. As the PRC increased from 1.6 to 4.6, the $\dot{W}_{Net+R+ETC}$is decreased. The increase is due to decreases in $\dot{W}_{Net\ and\ GT}$, and no significant energy can be recovered by the steam cycle, ETC. When the PR_C exceeds 4.6, the $\dot{W}_{Net+R+ETC}$ increases. Despite the decrease in the $\dot{W}_{Net\ and\ GT}$ at higher PR_C, the amount of energy recovered by the steam cycle and the ETC has increased the $\dot{W}_{Net+R+ETC}$.

Figure 14 and Figure 15 show that there is insufficient exhaust pressure to drive the radial turbine at PR_C <5 and at PR_C <5, meanwhile, at PR_C > 25, the diminishing returns as the system faces aerodynamic choking. Consequently, the recommended optimal deployment range for the system is $10 \leq PR_C \leq 25$**.** Also, there is a potential severe penalty of excluding the ETC or operating outside this range.

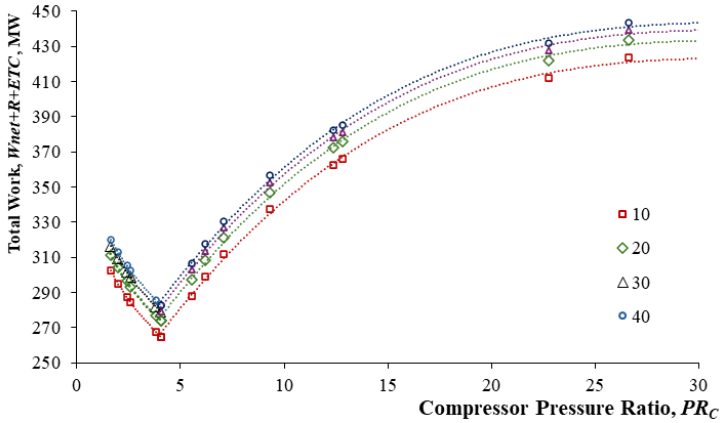

Figure 16. Total work of the system, $\dot{W}_{Net+R+ETC}$ for various compressor pressure ratio, PR_C and steam turbine pressure ratio, PR

3.5 Overall System Performance

The effect of recovered energy on the total Overall Cycle Efficiency of the system, $\eta_{Net+R+ETC}$at, at various PR_C and PR values is shown in Figure 17, where a similar trend is observed to that in Figure 16. This similar trend is due to the $\eta_{Net+R+ETC}$ ratio being higher for the $\dot{W}_{Net+R+ETC}$ and the $\dot{Q}_{Com}$. Comparing η for the baseline gas turbine with that of the energy recovery system can help analyse the contribution of recovered energy to the gas turbine system. Figure 18 illustrates the baseline η_{Net}, η_{Net+R}, and $\eta_{Net+R+ETC}$ at various PR_C at a combustion temperature DT = 1000 K. This figure shows that η generally decreases as PR_C increases, due to the high energy required to drive the compressor, except for $\eta_{Net+R+ETC}$. A single-stage energy recovery via a steam cycle can increase energy by less than 10%. A further increase in η can be achieved by installing an ETC (mechanical energy recovery system) downstream of the heat exchanger in the steam cycle. Although the ETC cannot recover energy at lower pressure ratios ($PR_C \leq 4.6$), it contributes significantly at higher PR_C. ETC can increase η by up to 80% at PR_C = 26.6 due to the downstream access pressure.

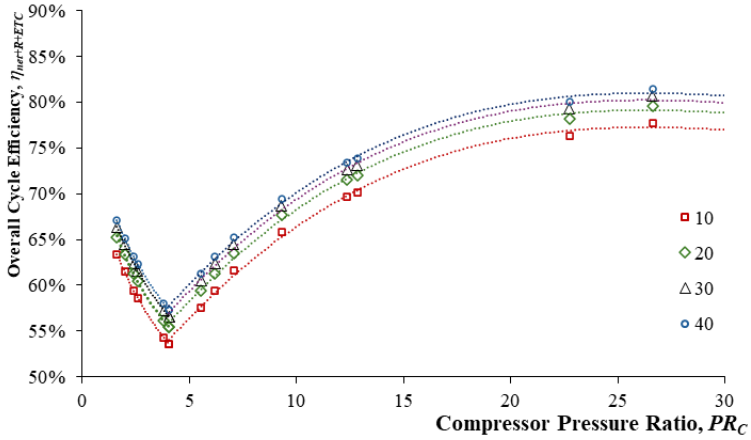

Figure 17. Overall cycle efficiency of the system, $\eta_{Net+R+ETC}$ for various compressor pressure ratio, PR_C and steam turbine pressure ratio, PR

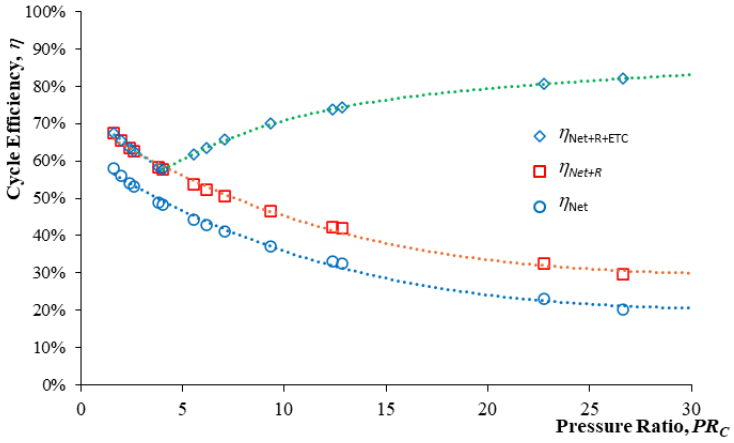

Figure 18. Comparison of cycle efficiency, η from baseline GT, steam recovery, ETC recovery at various pressure ratios, PR_C for DT = 1000 K

The losses for all major components are calculated and presented in the previous section, along with a comprehensive analysis of the Exergy Destroyed, $\dot{E}_D$ for each component. The $\dot{E}_D$ summary is shown in Figure 19 for various PR_C at DT= 1000 K. The Exergy Destroyed in the Gas Turbine, $\dot{E}_{D,GT}$ is the sum of the exergy destroyed by the Compressor, Combustor, and Turbine. Figure 19 shows that the $\dot{E}_{D,GT}$ contributes the highest $\dot{E}_D$ in the system, followed by the $\dot{E}_{D,R}$, and $\dot{E}_{D,ETC}$. The available recovered energy in the exhaust increases with higher PR_C. Although more energy can be converted into useful work by the ETC, Figure 19 shows that the $\dot{E}_{D,ETC}$ is higher than the $\dot{E}_{D,R}$ when the PR_C is greater than 20.

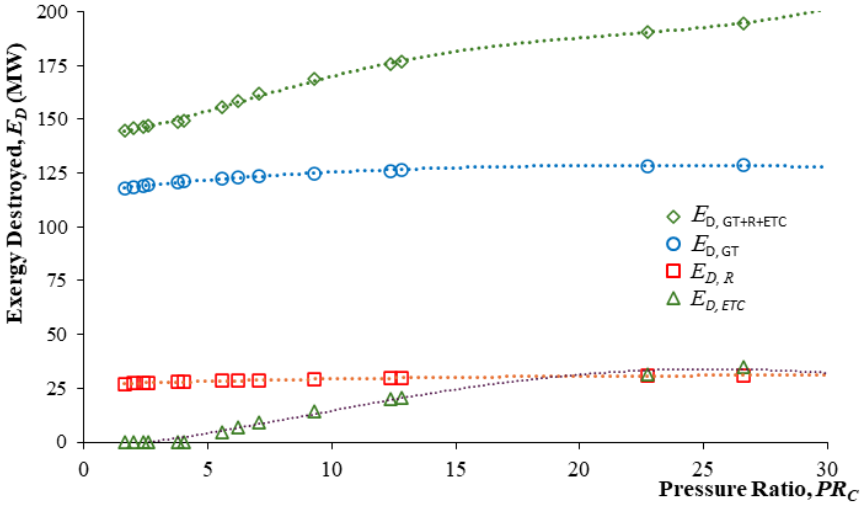

Figure 19. Exergy destroyed for baseline GT, steam recovery, ETC recovery at various pressure ratios, PR_C for DT = 1000 K

Exergy balance analysis is used to track exergy throughout the overall system. Figure 20 depicts the exergy rate balance analysis for the system. The primary source of exergy for the system, $\dot{E}_{Com}$, is the combustion of natural gas. The useful energy that can be converted by this $\dot{E}_{Com}$ is represented by $\dot{W}_{Net+R+ETC}$, which is the net power output of the gas turbine, the steam turbine, and the ETC. The net exergy exhaust loss, $\dot{E}_{D,Exhaust,}$ is the energy loss in the exhaust and was calculated as the difference between the exergy at the compressor inlet, $\dot{E}_{in}$, and the exergy at the ETC outlet, $\dot{E}_{out}$. Figure 20 shows that the $\dot{E}_{D,Exhaust}$ decreases as the PR_C increases because more exhaust energy is converted into useful work by the ETC. Finally, the accumulated exergy, denoted $\dot{E}_{Stored}$, represents the unused energy in the system and increases as the PR_C is increased. The $\dot{E}_{Stored}$ is a low-quality energy loss, and it becomes more significant when the PR_C exceeds 13 due to the higher exergy in that operating condition.

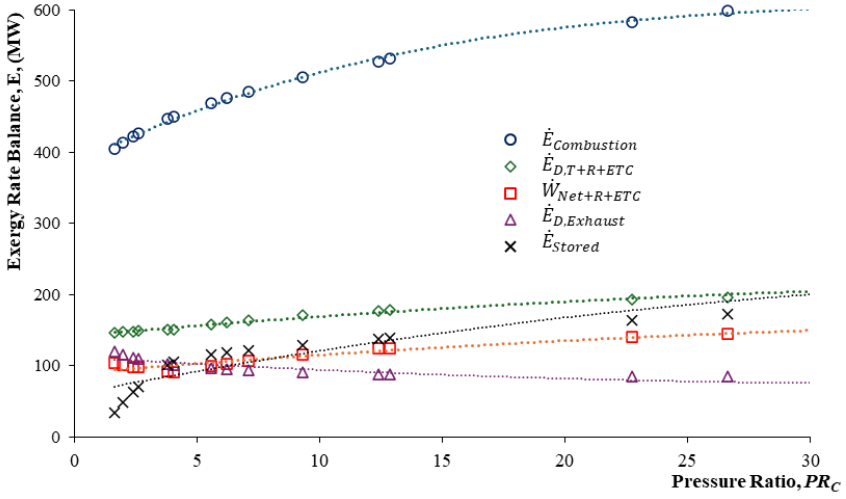

Figure 20. Exergy rate of balance at various pressure ratios, PR_C for DT = 1000 K

The overall system exergetic efficiency, $\eta_{II,}$ represents the effectiveness of the system in converting the input energy into useful work. The baseline of $\eta_{II,GT}$ is shown in Figure 11 for three (3) DT. In Figure 21, the effect of $\eta_{II,System}$ at DT= 1000 K was selected to compare η_{II} effect on energy recovery across varying PR_C. In general, the baseline gas turbine efficiency decreases sharply with increasing PR_C, falling below 10% at high PR_Cs. In contrast, the energy recovery system maintains a significantly higher and more stable efficiency (~50%) by utilising waste heat through steam generation and the ETC. Subsequently, the $\eta_{II,System}$ is higher than the $\eta_{II,GT}$ where the recovery mechanisms effectively offset the $\dot{E}_D$.

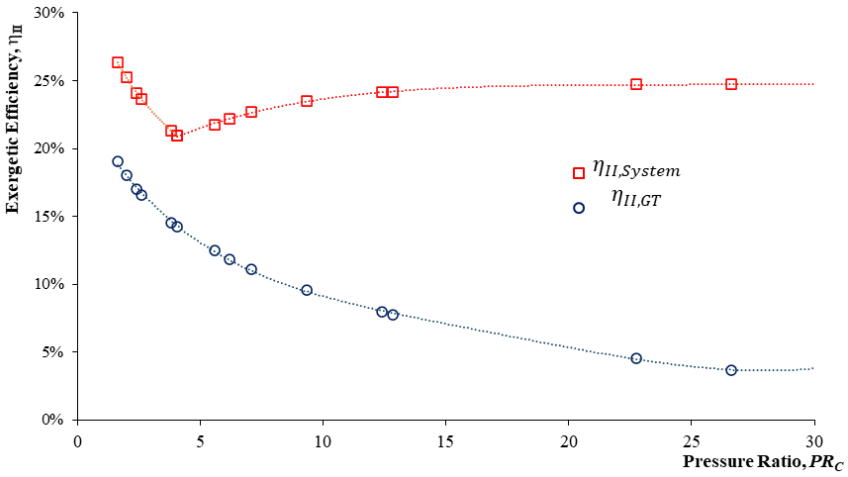

Figure 21. Overall system exergetic efficiency, $\eta_{II,system}$

3.6 Regenerative Cycle

The wasted exhaust exergy can be regenerated within the system, thereby increasing the η_{II}. The RC can be used to reduce the inlet exergy in combustion by increasing the combustion inlet temperature, as per $\dot{E}_{Com}$. A heat exchanger can be added between the HPC outlet and the combustion chamber. Figure 22 compares the required rate of heat regeneration, $\dot{Q}_{Regen}$, with the $\dot{E}_{Exhaust}$. The $\dot{Q}_{Regen}$ decreases as the PR_C increases and approaches zero at higher PR_C values, because the HP_C exit temperature increases. The PR_C is less than 6.2, and the $\dot{E}_{Exhaust}$ is less than the $\dot{Q}_{Regen}$. Thus, the exergy is limited; subsequently, the $\dot{Q}_{Regen} = \dot{E}_{Exhaust}$ in this region.

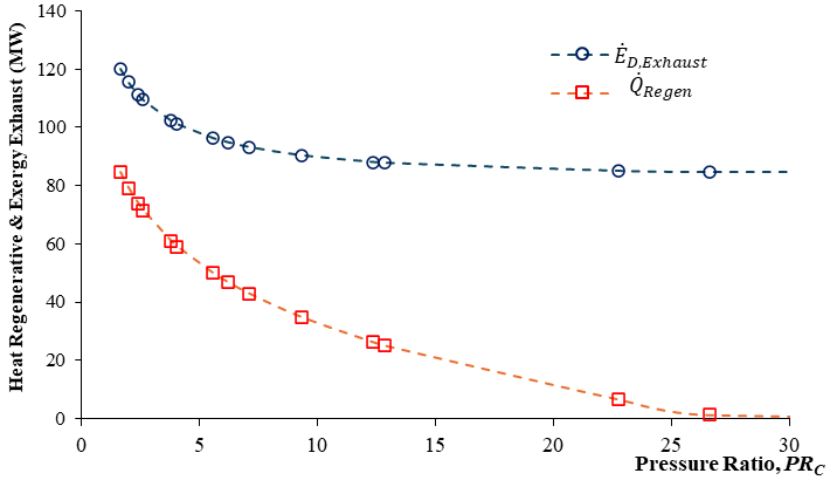

Figure 22. Rate of regenerative energy, $\dot{Q}_{Regen}$ and exhaust exergy $\dot{E}_{D,\,Exhaust}$ at various pressure ratios, PR_C for DT = 1000 K

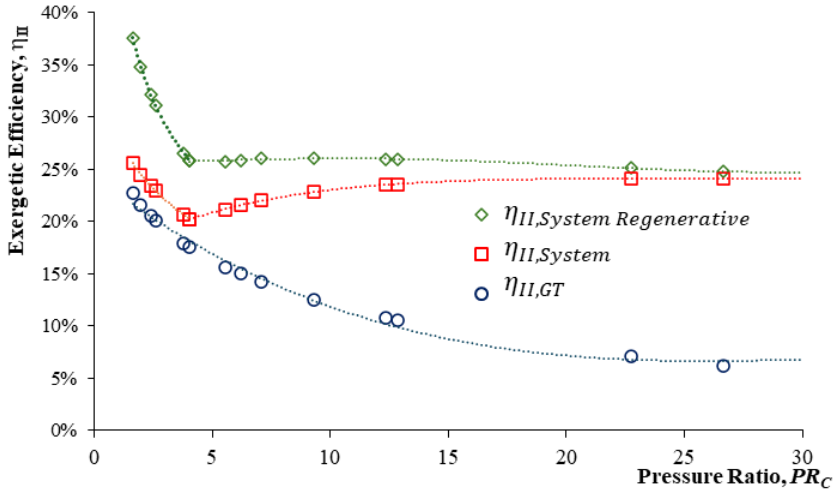

Figure 23. Overall system exegetic efficiency, η_{II}

The regenerative heat from the exhaust into the combustion chamber inlet has reduced $\dot{E}_{Com}$ and $\dot{E}_D$ by reducing the combustion chamber temperature difference. Figure 23 shows the comparison of the Exegetic Efficiency of the system, $\eta_{II,System}$, with the regenerative process, $\eta_{II,System\ Regenerative}$ and the baseline $\eta_{II,GT}$. The reduction in $\dot{E}_{Com}$ and $\dot{E}_{D,Com}$ had a significant impact on the overall system at the lower PR_C, with most of the exergy being utilised. Figure 23 shows that the $\eta_{II,System\ Regenerative}$ has increased by up to 10% compared to the $\eta_{II,system}$. However, that increment is not viable because of low PR_C region. The impact of $\eta_{II,System\ Regenerative}$ is less than 5% and the implication is reduced as the PR_C is increased. The results of the exergy rate balance sheet in terms of exergy magnitudes on a rate basis in Table 4. The table summarizes the results at the PR_C = 27 and the mass flow rate of 200 kg/s. The net Exergy supplied by the fuel combustion is 599 MW. The net disposition of exergy by the system including the waste energy recovery components is 144.9 MW which represents 24.5%. The total of Exergy destroyed at the operating condition is 455 MW which represents 75.5% of exergy supplied.

Table 4. Exergy balance sheet at PR_C = 27

Net Exergy through the Combustion, $E_{Combustion}$	599 MW	(100%)
Disposition of Exergy:		
Net Power Gas Turbine Cycle, $W_{Net,GT}$	37 MW	6.2%
Net Power Rankine Cycle, $W_{Net,Rankine}$	13.6 MW	2.3%
ETC Power, W_{ETC}	94.3 MW	15.7%
Regenerative Heat, $\dot{Q}_{Regen}$	1.95 MW	0.3%
Sub Total	144.9 MW	(24.5%)
Exergy Destroyed from Gas Turbine, $E_{D,GT}$ Compressor, Combustor & Turbine	128.8 MW	(21.5%)
Exergy Destroyed Steam Cycle, $E_{D,Steam}$	33.4 MW	(5.6%)
Exergy Destroyed ETC, $E_{D,ETC}$	34.8 MW	(5.8%)
Exergy Destroyed in Exhaust, $E_{D,Exhaust}$	85 MW	(14.2%)
Exergy Destroyed in the System, $E_{D,System}$	173 MW	(28.9%)
Sub Total Exergy Destroyed	455 MW	(75.5%)

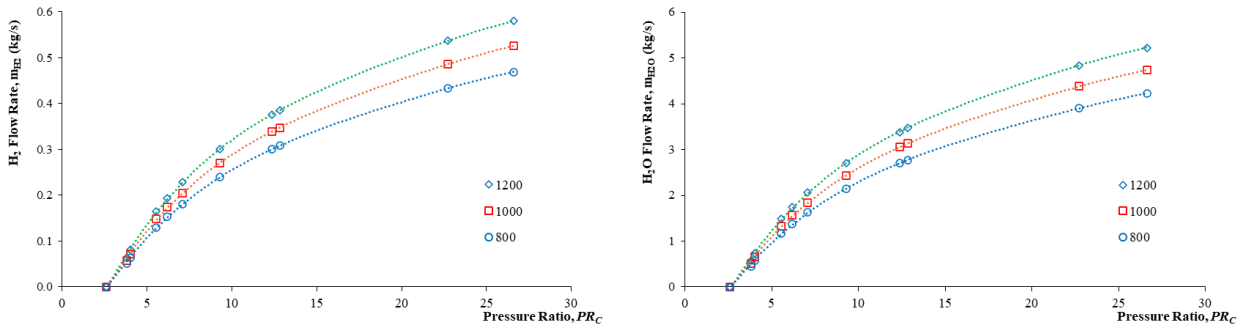

(a) H_2 Flow Rate (b) H_2O Supplied rate

Figure 24. H_2 production, $\dot{m}_{H_2}$ and H_2O supply rate in electrolysis process $\dot{m}_{H_2O}$

3.7 Hydrogen Production

The previous sections have presented the energy conversion and utilisation of the fuel. The fuel's exergy was converted into useful work, and it was shown that $\eta_{II\ (System\ Regenerative)}$ can be increased by nearly 90% in the system. Despite the high energy conversion efficiency, the system relies on natural gas, a non-sustainable, depleting hydrocarbon resource. Thus, a sustainable fuel such as H_2 can replace natural gas in the gas turbine system. The recovered energy from the system can be converted into hydrogen gas. The electrical energy recovered by the ETC was used to power the electrolyser that will produce hydrogen gas from the water supply. Figure 24 (a) shows the rate of hydrogen gas, $\dot{m}_{H_2}$, that can be produced from the electrolysis process, and Figure 24 (b) shows the water flow rate, $\dot{m}_{H_2O}$, to produce H_2. The electrical energy from the ETC was used to generate the electrolysis process. Since the ETC can only operate when the PR_C is greater than 5.0, the amount of Hydrogen production follows the ETC power trend: as the PR_C increases, $\dot{m}_{H_2}$ increases.

3.8 Exergoeconomic Analysis

Exergoeconomic analysis was conducted in this study to evaluate the economic consequences of exergy and irreversibility, as well as the potential revenue from H_2 production. Figure 25 shows that the Cost of Exergy, $\dot{c}_E$, for Natural gas varies between \$1727 per hr and \$1939 per hr, indicating the effective operation of the gas turbine at higher PR_C. The result is compatible with the commercial gas turbine performance data sheet shown in Table 1, where the $\dot{c}_E$ of

the natural gas fuels is less than $2000. Quantifying exergy destruction costs provides a rational basis for identifying cost-effective design improvements for the gas turbine system. Figure 25 shows that the increase in the Cost of Exergy Destroyed, $\dot{c}_{E,D}$, exceeds that in $\dot{c}_E$ as the PR_C increases, indicating a higher potential cost in this region. Thus, the gas turbine designer shall consider a higher-thermal-efficiency system, as proposed in this study. Cost of Exergy Recovered, $\dot{c}_{E,R}$ determines the offset economic value of waste exergy relative to the economic value of useful exergy. Figure 25 shows that $\dot{c}_{E,R}$ has a higher incremental value than $\dot{c}_{E,D}$, demonstrating a significant economic benefit from integrating the energy recovery system into the gas turbine power plant.

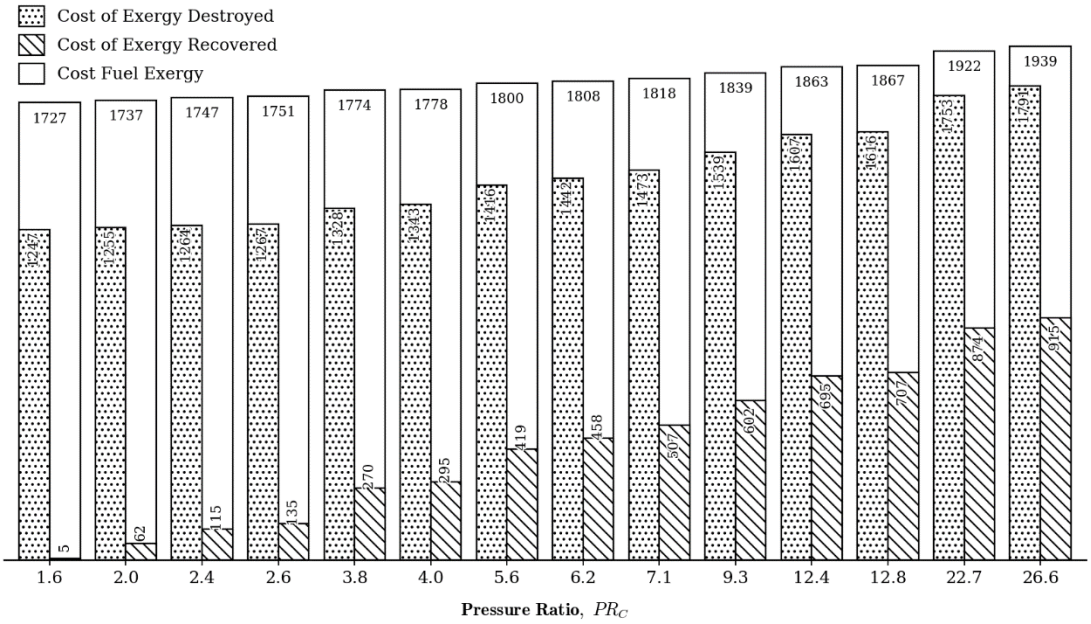

Figure 25. Cost of exergy, $\dot{c}_E$, cost of exergy destroyed, $\dot{c}_{E,D}$ and cost of exergy recovered, $\dot{c}_{E,R}$ from the gas turbine

Integrating energy recovery will increase the system's Capital Expenditure (CAPEX). However, this analysis focuses solely on the Operational Expenditure (OPEX) related to fuel consumption. Figure 26 shows the fuel cost of electricity, $\dot{c}_e$ from the gas turbine recovery system. The $\dot{c}_e$ is higher at lower PR_C because less exergy is recovered. As the PR_C exceeds 5.0, a significant reduction $\dot{c}_e$in ce is observed, from $23 per MWhr to $13 per MWhr. The reduction is because higher E_D can be recovered at a higher PR_C. The actual fuel cost of electricity from gas turbine data ($\dot{c}_{e,GT\ Data}$) is shown in Table 1, where almost all the $\dot{c}_e$ for commercial gas turbines are between $20 per MWhr and $25 per MWhr. The exergy recovery system could reduce $\dot{c}_e$ up to 50% compared to current costs.

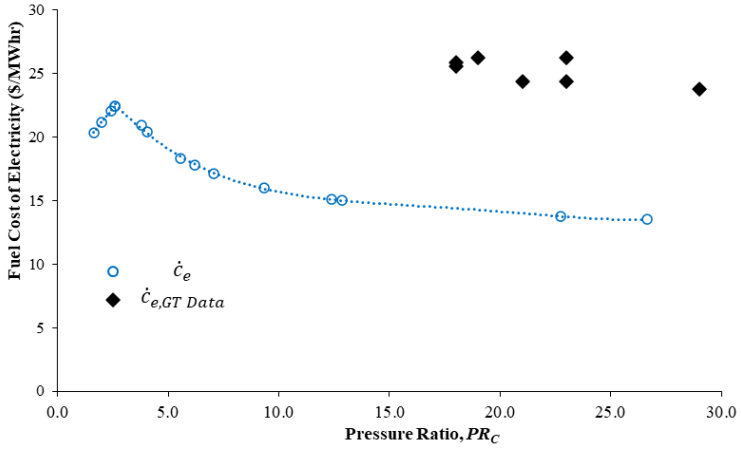

Figure 26. Fuel cost of electricity, $\dot{c}_e$ and fuel cost of electricity from commercial gt, $\dot{c}_{e,GT\ Data}$

The hydrogen was produced by electrolysis powered by the recovered exergy of the ETC. Figure 27 shows that the cost of hydrogen production, $\dot{c}_{H_2}$, produced from the fuel exergy varies: it is approximately $3.4 per kg at lower PR_C and reduces to approximately $0.4 per kg at $PR_C \geq 25$. The result demonstrates that WtH production from electrolysis powered by recovered exergy at higher PR_C is more effective than by-product hydrogen from Chlor-Alkali methods, as depicted in Table 2. Apparently, the improvement in the $\dot{c}_{H_2}$is due to the recovered exergy increases at higher PR_C; subsequently, more exergy can be used to produce $\dot{m}_{H_2}$. Moreover, additional revenue can be obtained by recovering the exergy destroyed in the gas turbine through the Hydrogen production. Figure 27 shows the hourly revenue from hydrogen

production ($\dot{R}_{H_2}$), indicating that $\dot{R}_{H_2}$ increases with PRC. However, there is no significant increase in $\dot{R}_{H_2}$ as the $PR_C \geq 25$, demonstrating the system's revenue limitations.

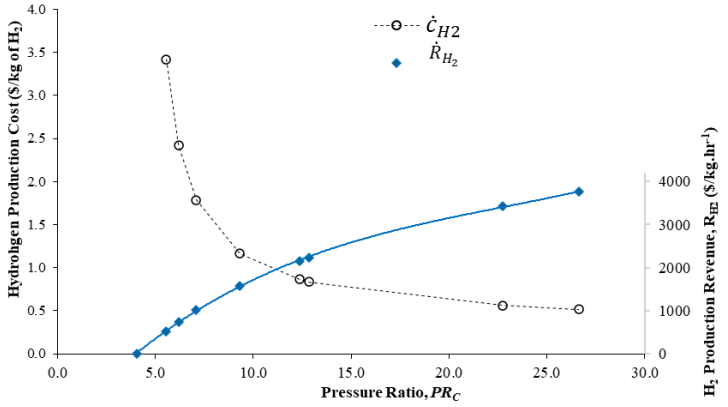

Figure 27.4 Cost of hydrogen production, $\dot{c}_{H_2}$ and revenue of H_2 production, $\dot{R}_{H_2}$

3.9 Parametric Sensitivity Analysis

The parametric sensitivity analysis was conducted to evaluate the robustness of the main parameters for this study, such as $\dot{m}_a$, ΔT and PR_C against $\eta_{ii,System\ Regenrative}$. The evaluation is centred around a nominal baseline operating condition (PR_C = 12.4, ΔT = 1000 K, $\dot{m}_a$ = 200 kg/s), which yields a baseline exergetic efficiency of 24%. The $\dot{m}_a$ varies from 150 to 250 kg/s, the ΔT varies from 800 K to 1200 K, and PR_C from 7 to 23. The results of this systematic variation are presented in the form of a Tornado chart in Figure 28 where the regenerative waste heat recovery system exhibits the highest sensitivity to the air mass flow rate. Varying the flow from 150 kg/s to 250 kg/s results in a symmetrical ±5% deviation from the baseline $\eta_{ii,System\ Regenrative}$. The combustor ΔT demonstrates an inverse and slightly asymmetrical impact on the e$\eta_{ii,System\ Regenrative}$. Reducing ΔT to 800 K improves efficiency by 3%, while increasing it to 1200 K reduces it by 2%. This reflects the increased exergy destruction inherent at higher combustion temperatures due to greater thermal irreversibility. Finally, the exergy modelling proves to be highly robust to changes in the pressure ratio. A substantial variation in PR_C from 7.1 to 22.7 induces a marginal ±1% fluctuation in the overall exergetic efficiency.

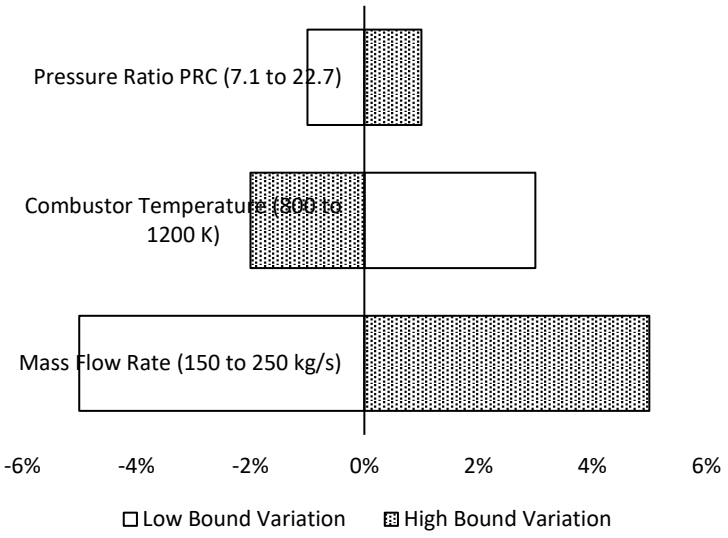

Figure 28 Parametric sensitivity analysis of the overall exergetic efficiency relative to the baseline operating condition (PR_C = 12.4, ΔT = 1000 K, $\dot{m}_a$ = 200 kg/s)

4. Conclusion

This study establishes a transformative, systems-level framework to enhance gas turbine power plants by synergistically integrating multiple waste-energy recovery systems. The developed thermodynamic model demonstrates that a cascading architecture, combining a CCPP, ETC, and a RC, can radically improve performance, elevating the system's exergetic efficiency from a baseline maximum of 11% to approximately 26%. The economic implications of this integration are profound. The model shows that recovered exergy can reduce electricity costs by up to 50%, significantly improving operational economics. Furthermore, by channelling the ETC's electrical output to on-site electrolysis, the system enables the production of WtH hydrogen at a cost as low as $0.3/kg. Hydrogen production not only creates a substantial additional revenue stream but also paves the way for integrating sustainable fuel synthesis directly into thermal power generation, thereby reducing the thermal power plant's carbon footprint. The optimal deployment range is $10 \leq PR_C \leq 25$ for the ETC

operating range, due to diminishing benefits at higher PR_C. Economically, failing to utilise the ETC eliminates the power source for the hydrogen electrolyser, completely losing the ~$3,500/hr revenue stream and increasing the specific fuel cost of electricity.

While derived from a robust theoretical model under steady-state, idealised assumptions, these results provide a compelling conceptual blueprint for the next generation of high-efficiency, low-carbon power plants. The significant gap between the modelled costs and current market realities underscores a tremendous opportunity for innovation. Future work should focus on experimental validation of this cascade recovery concept in a pilot-scale facility, the development of advanced control strategies for transient operation, and a full life-cycle techno-economic analysis that incorporates capital costs to demonstrate commercial viability. This work ultimately charts a clear course for overcoming the inherent inefficiencies of gas turbines, maximising useful work output, and advancing towards more sustainable and economically competitive thermal energy systems.

Acknowledgements
We would like to thank and acknowledge Universiti Teknologi MARA (UiTM), Malaysia, for providing laboratory facilities for this project.

Funding
This study was not supported by any grants from funding bodies in the public, private, or not-for-profit sectors.

Declaration of Competing Interest
The author declares no conflicts of interest.

CRediT Authorship Contribution Statement
N. A. Mohd Iskandar: Methodology; Data curation; Formal analysis; Visualisation; Writing - original draft
A. M. I. Mamat: Conceptualisation, Validation; Formal analysis; Writing - review & editing; Supervision

Availability of Data and Materials
The data supporting this study's findings are available on request from the corresponding author.

Ethics Declarations
This study did not involve human participants or animals. Ethical approval was therefore not required.

Generative Artificial Intelligence Declarations
The authors claim that artificially intelligent-assisted technologies, such as generative AI, were not used to generate content, ideas, or theories. We have just utilised AI to enhance readability and refine the language. This was used with extreme human control and oversight. The authors take full responsibility for reviewing and approving the content.

References
[1] M. M. Rahman, T. K. Ibrahim, and A. N. Abdalla, "Thermodynamic performance analysis of gas-turbine power-plant," *International Journal of Physical Sciences*, vol. 6, no. 14, pp. 3539-3550, 2011.
[2] L. Mustafa, R. Ślefarski, and R. Jankowski, "Thermodynamic analysis of gas turbine systems fueled by a CH4/H2 mixture," *Sustainability* (Switzerland), vol. 16, no. 2, p. 531, 2024.
[3] J. M. Michael and N. S. Howard, *Fundamentals of engineering thermodynamics*, (fifth edition). England: John Wiley & Sons Inc., 2021.
[4] R. S. Mishra and A. Singh, "Thermodynamic (Energy-Exergy) analysis of combined cycle gas turbine power plant (CCGT) for improving its thermal performances," *International Journal of Research in Engineering and Innovation*, vol. 1, no. 4, pp. 9-24, 2017.
[5] V. S. Reddy, S. C. Kaushik, S. K. Tyagi, and N. Panwar, "An approach to analyse energy and exergy analysis of thermal power plants: A review," *Smart Grid and Renewable Energy*, vol. 1, no. 3, p. 143, 2010.
[6] S. Dai, X. Zhang, and M. Luo, "A novel data-driven approach for predicting the performance degradation of a gas turbine," *Energies* (Basel), vol. 17, no. 4, p. 781, 2024.
[7] A. Almutairi, P. Pilidis, and N. Al-Mutawa, "Energetic and exergetic analysis of combined cycle power plant: Part-1 operation and performance," *Energies* (Basel)., vol. 8, no. 12, pp. 14118-135, 2015.
[8] R. K. Bhargava, M. Bianchi, L. Branchini, A. De Pascale, and V. Orlandini, "Organic Rankine cycle system for effective energy recovery in offshore applications: A parametric investigation with different power rating gas turbines," in *Proceedings of the ASME Turbo Expo*, vol. 56673, p. V003T20A004, 2015.
[9] S. O. Oyedepo and A. B. Fakeye, "Electric power conversion of exhaust waste heat recovery from gas turbine power plant using organic Rankine cycle," *International Journal of Energy and Water Resources*, vol. 4, no. 2, pp. 139-150, 2020.
[10] S. Kumar, "Performance optimization of combined cycle power plant considering various operating parameters," *Journal of Mechanical Engineering*, vol. 18, no. 1, pp. 21-38, 2021.
[11] N. Dev, Samsher, S. S. Kachhwaha, and R. Attri, "GTA modeling of combined cycle power plant efficiency analysis," *Ain Shams Engineering Journal*, vol. 6, no. 1, pp. 217–237, 2015.

[12] Ansaldo, "Ansaldo GT36," Ansaldo GT36 Brochure. Accessed: Nov. 26, 2025. [Online]. Available: https://www.ansaldoenergia.com/offering/equipment/turbomachinery/gt36
[13] Ansaldo Energia, "*Ansaldo GT36 Brochure*," 2023.
[14] G. Electric, "*7EA gas turbine fleet data*," 2020.
[15] G. Electric, "*7HA.01 product specifications*," 2022.
[16] General Electric, "*GE 7HA.03 product card*," 2023.
[17] GE, "*GE 9F.05 Technical guide," GE 9F.05 technical guide*. Accessed: Nov. 26, 2025. [Online]. Available: https://www.gevernova.com/content/dam/gepower-new/global/en_US/downloads/gas-new-site/products/gas-turbines/9f-fact-sheet-product-specifications.pdf
[18] G. Electric, "*LM2500 marine gas turbine*," 2023.
[19] GE, "*GE LM6000," GE LM6000 technical specifications*. Accessed: Nov. 26, 2025. [Online]. Available: https://www.gevernova.com/gas-power/products/gas-turbines/lm6000
[20] Kawasaki, "Kawasaki M7A-03," *Kawasaki M7A-03 product sheet*. Accessed: Nov. 26, 2025. [Online]. Available: https://global.kawasaki.com/en/corp/sustainability/environment/consideration/pdf/item_2021_13_e.pdf
[21] MHI, "Mitsubishi M501JAC," *MHI J-series performance data*. Accessed: Nov. 26, 2025. [Online]. Available: https://www.mhi.com/finance/library/annual/pdf/report_2023.pdf
[22] Ltd. Mitsubishi heavy industries, "*M701F4 gas turbine performance data*," 2021.
[23] P. & Whitney, "*FT8 MOBILEPAC® gas turbine specifications*," 2023.
[24] Rolls-Royce, "*Rolls-Royce RB211," Rolls-Royce RB211 industrial specs*. Accessed: Nov. 26, 2025. [Online]. Available: https://www.rolls-royce.com/products-and-services/civil-aerospace/widebody/rb211-524gh-and-t.aspx#/
[25] R.-R. H. plc, "*Trent 60 industrial gas turbine*," 2023.
[26] H. O. Egware and A. I. Obanor, "The investigation of an SGT5-2000E gas turbine power plant performance in Benin City based on energy analysis," *Energy Conversion and Management: X*, vol. 16, p. 100316, 2022.
[27] Siemens, "*Siemens SGT6-8000H," Siemens H-class datasheet*. Accessed: Nov. 26, 2025. [Online]. Available: https://www.siemens-energy.com/global/en/home/products-services/product/sgt5-8000h.html#/
[28] W. Zhuge, L. Huang, W. Wei, Y. Zhang, and Y. He, "Optimization of an electric turbo compounding system for gasoline engine exhaust energy recovery," in *SAE 2011 World Congress and Exhibition*, no. 2011-01-0377, 2011.
[29] D. T. Bălănescu and V. M. Homutescu, "Performance analysis of a gas turbine combined cycle power plant with waste heat recovery in organic Rankine cycle," *Procedia Manufacturing*, vol. 32, no. 1, pp. 520–528, 2019.
[30] J. Wang, Z. Lu, M. Li, N. Lior, and W. Li, "Energy, exergy, exergoeconomic and environmental (4E) analysis of a distributed generation solar-assisted CCHP (combined cooling, heating and power) gas turbine system," *Energy*, vol. 175, pp. 1246-1258, 2019.
[31] Z. Stępień, "A comprehensive overview of hydrogen-fueled internal combustion engines: Achievements and future challenges," *Energies*, vol. 14, no. 20, p. 6504, 2021. doi: 10.3390/en14206504.
[32] G. Tsatsaronis, "Thermoeconomic analysis and optimization of energy systems," Progress in energy and combustion science, vol. 19, no. 3, pp. 227-257, 1993.
[33] BloombergNEF, "*Hydrogen market outlook*," 2023. [Online]. Available: https://about.bnef.com/blog/hydrogen-market-outlook-2023/
[34] U.S. Department of Energy, "*H2A Hydrogen production analysis*," 2023. [Online]. Available: https://www.hydrogen.energy.gov/h2a_production.html
[35] S. G. C. Insights, "*Chlor-Alkali market report*," 2023. [Online]. Available: https://www.spglobal.com/commodityinsights/en/ci/products/chlor-alkali-market-report.html
[36] U.S. Energy Information Administration, "*Natural gas spot prices*," 2023. [Online]. Available: https://www.eia.gov/naturalgas/
[37] A. Arsalis, "Thermodynamic modeling and parametric study of a small-scale natural gas/hydrogen-fueled gas turbine system for decentralized applications," *Sustainable Energy Technologies and Assessments*, vol. 36, 2 p. 100560, 2019.
[38] B. B. Skabelund, C. D. Jenkins, E. B. Stechel, and R. J. Milcarek, "Thermodynamic and emission analysis of a hydrogen/methane fueled gas turbine," *Energy Conversion and Management: X*, vol. 19, p. 100394, 2023.
[39] International Energy Agency, "*Global hydrogen review*," 2023. [Online]. Available: https://www.iea.org/reports/global-hydrogen-review-2023
[40] S. G. C. Insights, "*Hydrogen market intelligence*," 2023. [Online]. Available: https://www.spglobal.com/commodityinsights/en/ci/products/hydrogen-market-intelligence.html
[41] U.S. Department of Energy, "*2023 Annual merit review and peer evaluation report*," 2023. [Online]. Available: https://www.hydrogen.energy.gov/pdfs/23001-hydrogen-program-amr-2023.pdf
[42] R. M. Institute, "*The value of turquoise hydrogen*," 2023, [Online]. Available: https://rmi.org/the-value-of-turquoise-hydrogen/
[43] U.S. Department of Energy, "*H2@Scale: Hydrogen production from nuclear power*," 2023. [Online]. Available: https://www.energy.gov/eere/fuelcells/h2scale
[44] I. N. Laboratory, "*Nuclear hydrogen production assessment*," 2023. [Online]. Available: https://inl.gov/hydrogen
[45] M. Moliere, J. N. Jaubert, R. Privat, and T. Schuhler, "Stationary gas turbines: An exergetic approach to part load operation*," Oil and Gas Science and Technology*, vol. 75, no. 10, p. 1, 2020.

[46] F. Khaldi and B. Adouane, "Energy and exergy analysis of a gas turbine power plant in Algeria," *International Journal of Exergy*, vol. 9, no. 4, pp. 399–413, 2011.
[47] Y. A. Cengel, *Heat and mass transfer: fundamentals and applications* / Yunus A. Çengel, Afshin J. Ghajar. 2015.
[48] M. Vedran, S. Perčić Gregor, and P.-O. Jasna, "Gas turbine upgrade with heat regenerator-numerical analysis of advantages and disadvantages," *Machines. Technologies. Materials*, vol. 12, no. 11, pp. 346-439, 2018.
[49] G. Bristowe and A. Smallbone, "The key techno-economic and manufacturing drivers for reducing the cost of power-to-gas and a hydrogen-enabled energy system," *Hydrogen* (Switzerland), vol. 2, no. 3, pp. 273-300, 2021.
[50] W. J. Chang, K. H. Lee, H. Ha et al., "Design principle and loss engineering for photovoltaic-electrolysis cell system," *ACS Omega*, vol. 2, no. 3, pp. 1009-1018, 2017.
[51] EIA, "*EIA Natural gas prices*," U.S Energy Information Administration. Accessed: Nov. 27, 2025. [Online]. Available: https://www.eia.gov/dnav/ng/ng_pri_sum_dcu_nus_a.htm